12-2016

Beta-Delayed Neutron Data and Models for SCALE

Kemper Dyar Talley
University of Tennessee, Knoxville, ktalley5@vols.utk.edu

To the Graduate Council:

I am submitting herewith a dissertation written by Kemper Dyar Talley entitled "Beta-Delayed Neutron Data and Models for SCALE." I have examined the final electronic copy of this dissertation for form and content and recommend that it be accepted in partial fulfillment of the requirements for the degree of Doctor of Philosophy, with a major in Energy Science and Engineering.

Mark L Williams, Major Professor

We have read this dissertation and recommend its acceptance:

Robert K. Grzywacz, Larry Townsend, Thomas Handler

Accepted for the Council:
Carolyn R. Hodges

Vice Provost and Dean of the Graduate School

(Original signatures are on file with official student records.)

Beta-Delayed Neutron Data and Models for SCALE

A Dissertation Presented for the

Doctor of Philosophy

Degree

The University of Tennessee, Knoxville

Kemper Dyar Talley

December 2016

To my friends and family without whom I would be adrift ...

Acknowledgements

Thank you ...

Mark Williams, my advisor, for his patience and direction in this process. His knowledge and direction has been invaluable.

Ian Gauld for the many conversations and his thoughts, questions, and his open door.

Robert Grywacz for teaching me nuclear physics for two semesters where I learned about the fundamentals. He originally directed me to Miernik's work.

William Wieselquist for development of the ORIGEN API and his help with programming which allowed me to implement various theories and experimental data.

Erik Olsen, Noah Birge, and Justin Willmert my fellow graduate students in this endeavor.

Witek Nazarewicz for his patience and his tutelage at the beginning this process. Without his immense knowledge and prodding I would not have learned as much. Thank you for helping even during a time when I did not know how to help myself.

Larry Townsend and Thomas Handler for their teaching and for agreeing to serve on my doctoral committee. I am grateful for your time and discussions.

Mark Godwin, my first physics teacher. Without your inspiration, teaching, and friendship I would never have decided to pursue a career in physics.

Emil Alexov, my first research mentor, at Clemson University. I'm grateful for the chance to learn the research and publishing process from him.

Finally I would like to thank Lee Riedinger, the director of the Bredesen Center for accepting me into the program and helping me find a mentor. His patience is perhaps greatest of all since we both expected this adventure to take much less time.

The road that stretches before our feet is a challenge to the heart long before it tests the strength of our legs.

-Thomas Aquinas

Abstract

Recent advancements in experimental and theoretical nuclear physics have yielded new data and models that more accurately describe the decay of fission products compared to historical data currently used for many applications. This work examines the effect of the adopting the Effective Density Model theory for beta-delayed neutron emission probability on calculations of delayed-neutron production and fission product nuclide concentrations after fission bursts as well as the total delayed neutron fraction in comparison with the Keepin 6-group model. We use ORIGEN within the SCALE code package for these calculations. We show quantitative changes to the isotopic concentrations for fallout nuclides and delayed neutron production after fission bursts on the order of a few percent. We also show that the changes are larger at small times for short lived fission products, and that corrections to the cumulative fission product yields has an impact upon the total delayed neutron fraction for ^{235}U [Uranium 235]. The effect of modeling the β_{2n} [beta delayed double neutron emission] decay mode is also studied but no significant changes from the single beta-delayed neutron emission is currently seen.

Table of Contents

List of Tables

List of Figures

List of Attachments

Accelerating a Metropolis Random Walk and Immersion-Method Saddle-Point Algorithms in Multidimensional Nuclear Potential-Energy Spaces.pdf

Chapter 1

Introduction

Advancements in nuclear theory from both *ab-initio* and phenomenological methods have yielded results that may be ready for implementation into nuclear engineering methods, but the process of evaluation continues to be a challenge. Thorough understanding of various nuclear models and their use to generate evaluated nuclear data is a task that is usually left to a relatively few expert evaluators, and the task can often be one that lasts a lifetime.

The entirety of this work deals with improvements in the understanding of processes surrounding nuclear fission by using phenomenological models. Specifically those issues concerning the yields of nuclides after fission and the subsequent beta-decay and possible neutron emission. While the theories introduced here also have implications for astrophysics, we will restrict ourselves to nuclear engineering applications. The goal of this work is implement new nuclear data obtained from recently developed phenomenological models into the nuclide transmutation code ORIGEN, which can be used to verify the data by comparison with experimentally measured nuclide concentrations.

My specific contributions include a quantitative representation of the changes in isotope production using the Effective Density Model calculations for delayed neutron emission as compared to ENDF/B. We also show a quantitative representation of the changes to delayed neutron production and total delayed neutron fraction. All simulations were done with ORIGEN utilizing fission bursts of ^{235}U, ^{238}U, ^{239}Pu with fast and 14 MeV fission spectra.

Considerable time has also been spent developing improvements in a nuclear physics code that deals explicitly with pathways for fission and the prediction of the production of nuclides after fission. The work makes improvements on various computations within the Finite Range Droplet Method.

My specific contributions accelerated the computation time for a metropolis random walk and the determination of saddle-points within an immersion method for multidimensional spaces. Performance analysis shows the overall computation time was decreased dramatically. To accomplish this within the Finite Range Droplet Method, we modernized codes from FORTRAN77 to FORTRAN 95, utilized OpenMP for parallel computation, and introduced various new methods. The methods included speeding up a search for minima, using binary formats instead of ASCII, implementing a new saddle point determination algorithm, introduction of simultaneous flooding, and a bounding box for calculations. For more details on advancements and contributions to those issues related to the work done in nuclear fission mass studies, the reader is directed to the attachment as this work will spend little time detailing that work [41].

1.1 Nuclear Data and Motivation

We must specify what we mean when we say that there are improvements to be made to the processes listed above. One clear and quantitative way to assess the effects of new theory and experimental data is to examine the current status of the nuclear data and compare it to any proposed changes. Accurate nuclear data is critical for many applications such as: reactor design and fuel cycle modeling, nuclear forensics, spent fuel storage, understanding astrophysical processes, and nuclear safeguards. The Evaluated Nuclear Data File (ENDF) is one of several comprehensive evaluated nuclear data libraries in the world, and is the primary source of nuclear reaction cross sections and other types of data used for nuclear analysis in the U.S. The most recent version is ENDF/B-VII.I[6] released in 2014. The ENDF/B format (which has also been adopted by other evaluated data files) is composed of several

sub-libraries. The sub-library for decay data is commonly referred to as File 8, and this file is based on experimental decay data in the Evaluated Nuclear Structure Data File (ENSDF) as well as various other evaluations and theoretical models where experimental nuclear data does not exist. Even though evaluations are the culmination of extensive work and verification, subsequent data testing is needed to identify data that needs improvement, and in a few cases may reveal errors due to incompatibility of data [12], improper implementation of theory, lack of accurate experimental data [7, 33], and even transcription errors [15]. This work will identify a few of these issues related to the topic of interest.

The specific data of critical importance for our purposes is the total energy available for beta-decay (Q_β), the independent and cumulative fission product yields (FPYs), and the probability of particular decay modes (branching ratios): beta-decay and neutron emission. In this work the Q_β is based on the 2003 Audi mass evaluation which was updated with newer experimental data from the following reference: [38]. The FPYs for ^{239}Pu are given by a Bayesian technique [17], and the FPYs for all other nuclides are based on the compilations of England and Rider of which part is reproduced in the appendix B.2 [10]. The two main sources of branching ratios for various beta-decay and neutron emission are experimental values from ENSDF where they are available and calculations from Kawano and Möller (based off of a QRPA Hauser-Feshbach model) when the experimental data is not available [16].

One of the outstanding problems in nuclear engineering is the incompleteness fission product data as well as the inclusion of antiquated data that may have significant problems in the data collection procedures compared to newer methods like the Versatile Array of Neutron Detectors at Low Energy (VANDLE) [22] and Modular Total Absorption Spectrometer (MTAS) [44]. This has led to newer data that contradicts older data from delayed neutron emission probabilities (P_n) and for the total energy produced from gamma rays, a major source of decay heat, which is the primary driver in meltdowns after a reactor has been scrammed like in Fukushima in 2011. Also many of the calculations are based on systematic

theories such as the Kratz-Hermann Formula (KHF) which may not be as accurate or reliable as newer theories [25, 28, 43].

There have also been several problems with the delayed neutron data in moving from ENDF/B-VI.8 to version ENDF/B-VII.0 that had resulted in a move back to ENDF/B-VI data for delayed neutrons [6]. Since then, the new ENDF/B-VII.1 was released and is used. However there are still issues with this decay data since the fission product yields have not been updated with any of these new decay data and thus are inconsistent. A few issues are based in the short lived delayed neutron emitters that are in groups 5 and 6 of the Keepin 6-group model as seen in the appendix B.3. In fact, the problem of properly modeling short lived fission products has been a challenge for many years [28]. This work will advance some of the knowledge on the problem by introducing a new theory that is more accurate as well as addressing a few of the problems with the cumulative yields. In regards to independent and cumulative yields in ENDF, the incompatibility of data has been recently studied [29]. Independent yields are direct yields per fission prior to any decay and cumulative yields are the yields per fission after any and all decays including delayed neutrons. Cumulative yields of longer lived nuclides, which can be measured experimentally, are directly affected by the decays of the nuclei produced in fission. However nuclide transmutation computations utilize independent yields, which should be consistent with the cumulative yields and decay data.

1.2 Nuclear Fission and Mass Tables

Nuclear fission produces a great range of nuclei that then undergo various decays as shown in Figures 1.1 and 1.2. There exist various approaches to modeling nuclear fission yields within nuclear theory, but one of the most prominent models that has been used in evaluations for ENDF by England and Rider is that of the Finite Range Droplet Method (FRDM) [27] developed by Möller et. al. This method combines the finite-range droplet model with various microscopic corrections that handle deformation and shell effects in order to make various

calculations of nuclear properties. This is also the method that is used for the prediction of the mass energy hyper-surface in the attached work on nuclear fission calculations.

One of the most important if not most important calculation is that of mass for nuclei. In our application this is also true since the mass of a specific nuclei directly influences the energetics of beta-decay and neutron emission. While there have been significant updates to individual databases and calculations, ENDF VII.I uses the 2003AME evaluation but sometimes employs models in other areas that are based off of older evaluations like those mentioned above. In order to reliably predict and evaluate nuclear data (especially delayed neutron data) it is important to understand what different mass models are being used by various theories so that the calculations can be compared fairly. The current iteration from Möller, FRDM(2012), compares some calculated masses to a few mass evaluations to give an idea for how much can change between those models.

Models like FRDM are necessary because the mass evaluations do not contain experimental measurements for masses for all nuclei produced by nuclear fission, and even for measured nuclei the uncertainties in mass will lead to uncertainties of other properties when they have not also be measured. In fact, some of the most prominent compilations like those of England and Rider use Möller's model when there were no experimental data available as shown in the appendix B.2. While experimental data is preferred and studies on nuclei further and further from stability are being studied at facilities around the world, those efforts take large amounts of time, effort, and funding. Also, there may also be set-backs such as the closing of Holifield Radioactive Ion Beam Facility at ORNL. During it's time many nuclei were studied, and in the most recent campaign more than 30% of the total cumulative fission yield of ^{238}U was studied [33]. Over time, all of this data will be made available for inclusion into data evaluations contained in ENDF. If the reader would like more information on FRDM, the attachment details it further as it was used extensively in that work.

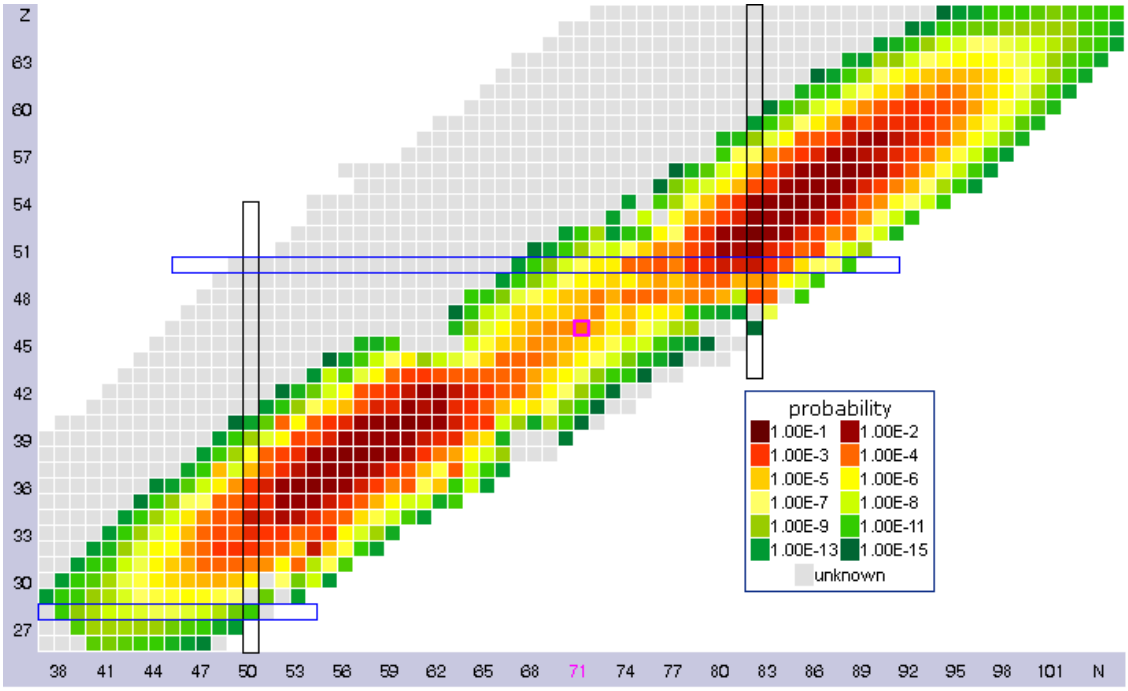

Figure 1.1: Cumulative FPYs for ^{235}U

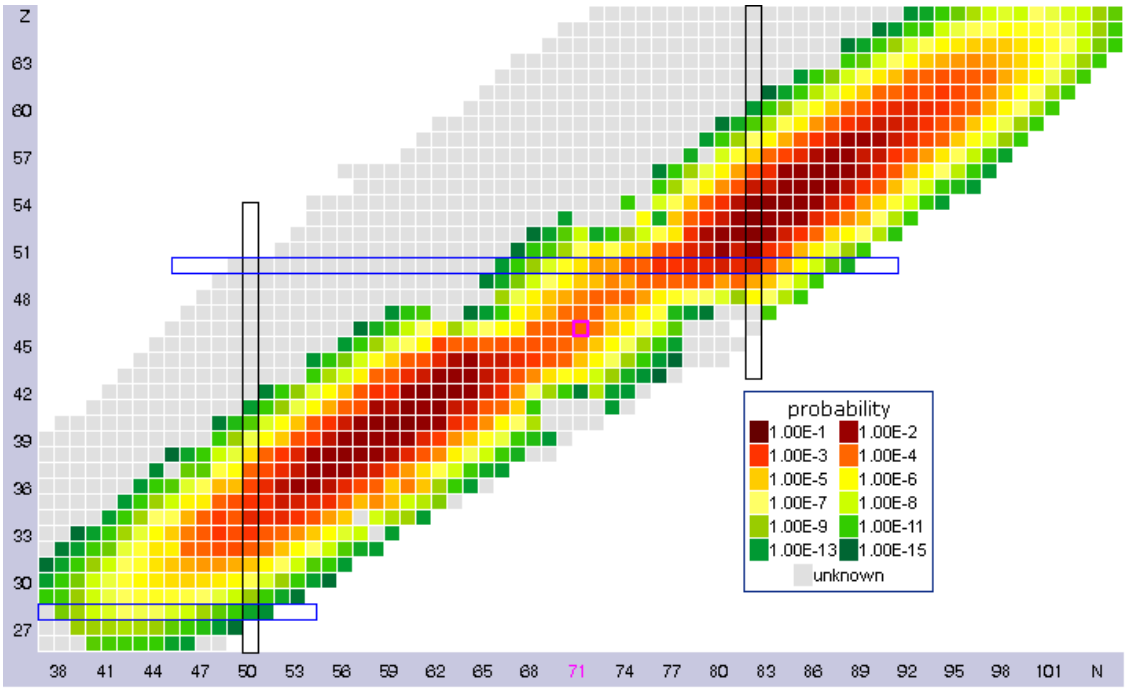

Figure 1.2: Cumulative FPYs for ^{239}Pu

1.3 Beta-Decay and Delayed Neutron Emission

The Interactive Chart of Nuclides at the National Nuclear Data Center (http://www.nndc.bnl.gov/chart/) allows users to quickly understand and see various nuclear data. In Figure 1.3 we see the dominant decay mode for all nuclides. Our region of interest can be shown in the FPYs of ^{235}U and ^{239}Pu in Figures 1.1 and 1.2.

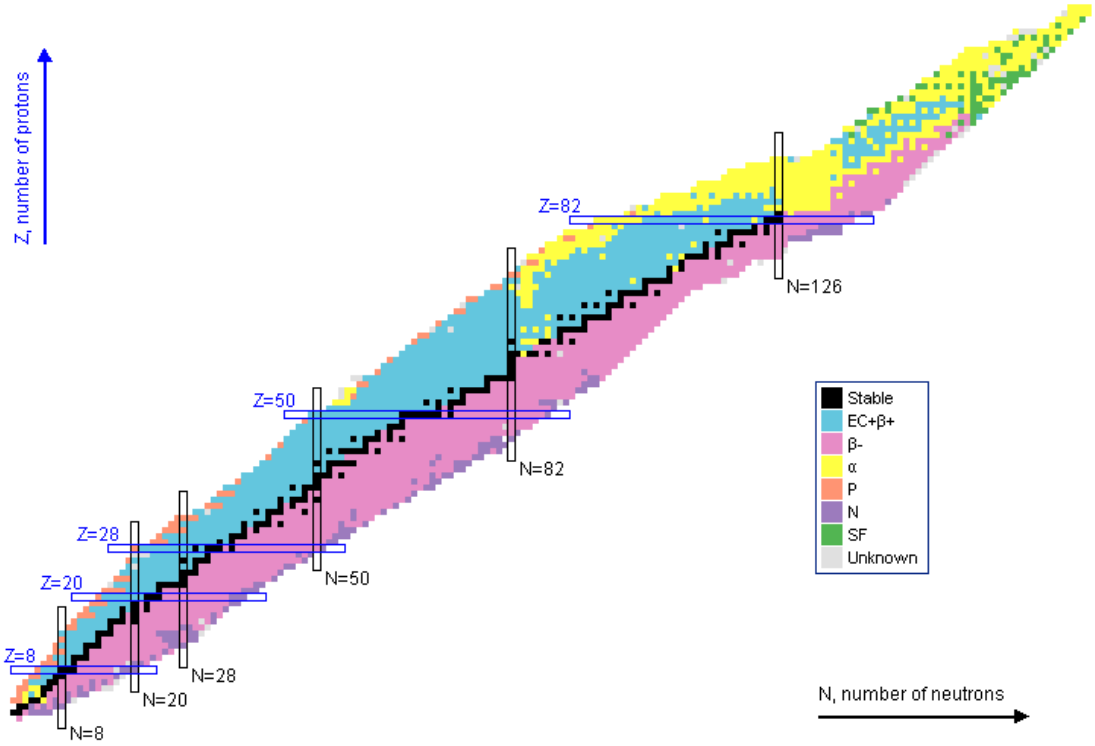

Figure 1.3: Dominant Decay Mode for All Nuclides

The dominant mode of decay for fission products is beta-decay. While fission product nuclei typically de-excite by beta-decay, there is also sometimes enough energy available in nuclei of very unstable nuclides for a neutron to be emitted. This particular neutron is called a beta-delayed neutron and is very important for reactor control. To put things in perspective, the fission products that undergo beta-decay account for around 4% of the total energy released in nuclear fission [8]. While prompt neutrons (neutrons that are emitted immediately after fission) account for a majority of the neutrons available to the reactor,

the total delayed neutron yield is still significant. This total number of delayed neutrons produced per fission can be described by the following equations:

$$\nu_d = \bar{\nu} * \beta \tag{1.1}$$

where $\bar{\nu}$ is number of the neutrons released per fission (prompt and delayed) and β is the fraction of neutrons that are delayed. For ENDF/B-IV ^{235}U ν_d is 0.01668 ± 0.00070 n/f and $\bar{\nu}$ is 2.43, which means that for every fission 0.01668 neutrons are expected to be delayed. The delayed neutrons appear over a time period of a few microseconds to 55 seconds (in the case of ^{87}Br) after fission occurs. The delayed neutron parameters and effect it has on reactors using point reactor kinetics can be found in any introductory nuclear engineering text. There are other sources for neutrons ((alpha,n) and photo neutrons), but this work is not explicitly concerned with those neutrons.

Beta-decay and subsequent neutron emission can be represented as such:

$$^{A}_{Z}X \Rightarrow ^{A}_{Z+1} Y + e^{-} + \bar{v_e} + Q \tag{1.2}$$

$$^{A}_{Z}Y \Rightarrow ^{A-1}_{Z} Y + n + Q \tag{1.3}$$

where X is commonly referred to as a precursor nuclei if the daughter nucleus Y undergoes neutron emission. The energy available to the reactor only excludes energy carried away by the anti-neutrino (v_e, which is not to be confused with the number of neutrons that are delayed, $\bar{\nu}$). It is also useful to express these relations in terms of Q_β and the neutron separation energy (S_n):

$$Q_\beta = ^{A}_{Z} M - ^{A}_{Z+1} M \tag{1.4}$$

$$S_n = ^{A}_{Z} M - ^{A-1}_{Z+1} M - ^{1}_{0} M_n \tag{1.5}$$

M represents the mass of the particular nuclei, and should not be assumed to be the same between any two given calculations since different mass tables could be used.

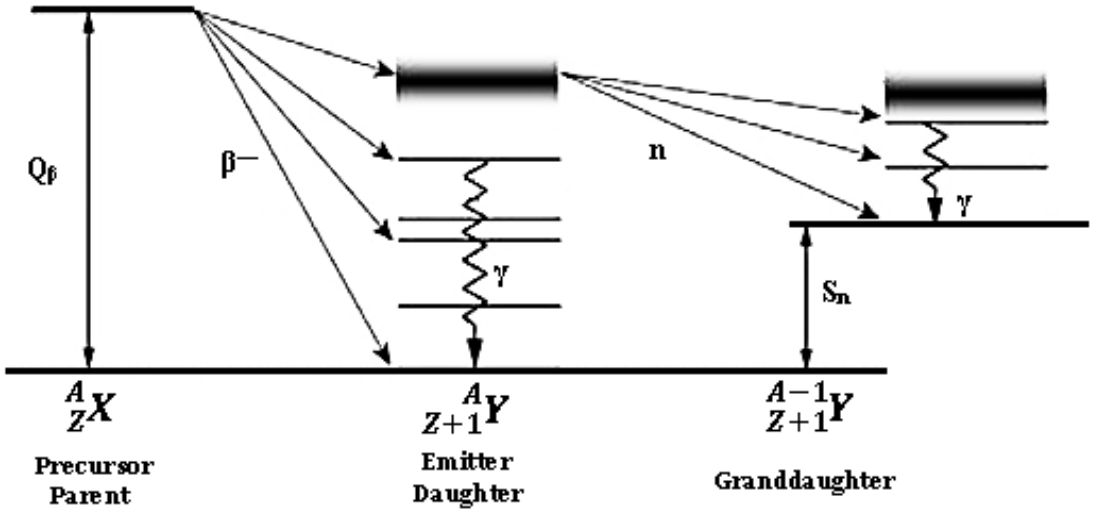

Figure 1.4: Schematic of Beta-Decay and Delayed Neutron Emission

Whenever Q_β for the parent nucleus is greater than zero, there is a probability of beta-decay (P_β). This decay can go into one of many excited states of the daughter nucleus. Additionally, if Q_β is greater than S_n, there is a probability of neutron emission (P_n). The picture can become even more complicated because the daughter nucleus may have the possibility of undergoing a further beta-decay which will compete with the decay via neutron emission. The reality is that any decay that is energetically favorable may occur, but the competition and complexity of decay between states typically means that one decay dominates the others. For many nuclei within our region of interest there is a significant branching ratio for multiple decay channels. There is also the possibility of multiple neutron emission if Q_β is greater than $S_{xn}; x \geq 2$.

Beta-decay often has a significant half-life on the order of a few milliseconds to minutes, and often the delayed neutron precursors will be binned into groups for nuclear engineering applications. This would split up β into many different β_i that would be summed to give β in equation 1.1. The most famous of which is the Keepin 6-group formulation. The constants for each group are empirical fits to the experimental data which should change with the neutron energy spectra. While there have been many advancements over the original Keepin 6-group formulation in 1965, there still remains work to be done. This work may motivate

an explicit precursor representation that should be possible with advancements in nuclear data, theory, and computation. Some of these tables that are reproduced in the Appendix.

In this common six group formulation the precursor that emits neutrons at the longest half-life (55.6 seconds) in group 1 is that of ^{87}Br which decays into ^{87}Kr. In principle the decay is into the excited state of krypton ($^{87}Kr^{*}$) above the neutron separation energy then it can undergo neutron emission to ^{86}Kr which is stable. If the decay is into the ground state of ^{87}Kr, it will continue to beta-decay until it reaches ^{87}Sr which is also stable. The probability that ^{87}Br will undergo beta-decay followed by neutron emission is 2.6% ($\%\beta_n^- = 2.6\%$).

In ENDF VII.IB, P_n is taken from experiments if available in ENSDF or the Pfeiffer et al. (2002PF04) [28] and for all other such cases calulations from Kawano and Moller are used [16]. This leads to 89 values from ENSDF, 9 values from 2002PF04, and 237 values from Kawano and Moller (QRPA-Hauser-Feshbach) for P_n. These calculations were done in 2008 and since that time a few new models have introduced improvements. It is worth noting that there are many QRPA(Quasi-particle Random Phase Approximation)Hauser-Feshbach values for P_n that are negligible. When those are taken out, one finds 350 precursors in ENDF/B-VII.1 as well as 155 multiple neutron emitters (non-zero $P_{xn}; x \geq 2$). One reference gives a value of 203 precursors in this fashion with 109 having some kind of measurement data [3]. This last point is at odds with the 163 experimental values cited in reference [25]. One of the most comprehensive works on delayed neutron precursors was a thesis by Brady which identified 271 important precursors using energetic arguments like those above [4]. These discrepancies are probably due to differing methods for calculating $Q_\beta - S_n \geq 0$ since those quantities depend on the selection of a specific mass table. It is usually assumed that Brady's identification of 271 precursors is the most reliable as it is cited in almost any evaluation on delayed neutrons.

It is important to make a clear remark about ENDF and the data that is being used as our default library, especially for the work presented in the following chapters. Even though ENDF VII.I is the most recent update, there is still uncertainty within the delayed neutron data. For that reason we will focus on comparing results to systematic theories like KHF

that are most comparable to the calculations done in the evaluations by England and Rider that were used for ENDF VI. ENDF VI results for delayed neutron data is based off of four sources: the England and Rider evaluation, the Background Radiation from Fission Pulses report [9], the third source is LA-UR-86-2693 from a meeting in 1986 on delayed neutrons that we could not find, but it is supposedly superseded by the last source: the Brady's thesis [4]. The ENDF-349 is reproduced in the appendix B.2 Also, since we are working within the SCALE framework and specifically with ORIGEN, the default data library for ORIGEN is ENDF-B/VII.1 which is also supplemented by other sources. More details about the ORIGEN libraries can be found in the SCALE documentation. More time will be spent on the specifics of that library and its data later. For now we will focus on the calculation of P_n from various models, including the one being newly implemented in ORIGEN, the Effective Density Model (EDM) introduced by Krystof Miernik [25].

Chapter 2

Methodology

This chapter will review the theory and the computational tools that are represented by this work. In Section 2.4 we review ORIGEN, the basic theory and computational methods employed to understand the decay processes after fission. The systematic formulation used for predictions of the probability of neutron emission in the England and Rider evaluation (ENDF-349) and it's updates concluding in the Brady thesis [4] are detailed in Section 2.2 for the Kratz-Herrmann formula (KHF). We also review the most recent phenomenological approach given in Section 2.3 the Effective Density Model (EDM).

In order to assess the changes that would be present with changes to ORIGEN's decay data libraries the ORIGEN Application Program Interface (API) developed by William Wieselquist was used. Documentation for the API can be found in the SCALE documentation, and I will only outline the key processes and developments used in this work in Section 2.4.3. Before moving on to the ORIGEN calculations it is important to advance some knowledge about the theories that will be compared: KHF, EDM, and QRPA Hauser-Feshbach.

The general flow of the methodology for calculations is as such:

1. Run simulation with default decay library for P_n - ENDF/B-VII.I (ENSDF experimental data and QRPA Hauser-Feshbach calculations)
2. Modify decay library with new data (EDM, KHF, Microscopic Theories, experiments, etc.)
3. Run simulation with new decay library
4. Compare results of isotopic concentrations and delayed neutron production between default and new library

The simulation in ORIGEN is done on fission bursts with the following isotopes and neutrons: ^{235}U fast, ^{238}U fast, ^{235}U 14 MeV, ^{239}Pu 14 Mev. The following selection criteria is applied throughout this work except where explicitly noted:
1. Nuclides relevant to fallout (found in Appendix C)
2. Nuclide concentrations (gram-atoms) $\geq$ 1E-10
3. Difference between model calculations $\geq 1\%$

A sample ORIGEN input deck can be found in the Appendix C.1

2.1 Beta-Delayed Neutron Emission Probability

As mentioned before for beta-delayed neutron emission to occur, Q_β must be larger than S_n of the daughter product. The probability of neutron emission can be represented in general by the following equation:

$$P_n = \frac{\int_{S_n}^{Q_\beta} \frac{\Gamma_n(E)}{\Gamma_{tot}(E)} S_\beta(E) f(Z+1, Q_\beta - E) dE}{\int_0^{Q_\beta} S_\beta(E) f(Z+1, Q_\beta - E) dE} \tag{2.1}$$

Where Γ_n is the neutron width, Γ_{tot} is the total state width, f is the Fermi integral, E is the excitation energy of the daughter nuclide, and S_β the beta-strength function.

The challenge of solving this equation largely depends on computing the β-strength function. Several macroscopic approaches have been carried out in the past that largely lie along the following lines: gross theory (statistical) [35], constant $S_\beta(E)$, and $S_\beta(E)$ proportional to the level density ($\rho(E)$). This work will focus a on the latter two approaches within the KHF and EDM models. It is important to also point out there have been many attempts since then to treat the β-strength function in a fully self-consistent microscopic manner but the application of this approach to nuclear engineering applications would be foolish at this time. In fact this work explored one of the most recent models and found it to be wholly unsuited for nuclear engineering applications without tremendous reworking of the data and theory [21]. In the approaches used by this work the following assumption is taken: for $E > S_n$ γ-decay from neutron-unbound levels is neglected or said in another way neutron emission is assumed to the dominant de-excitation path. This means that the quantity Γ_n/Γ_{tot} is equal to one. Thus equation 2.1 becomes:

$$P_n = \frac{\int_{S_n}^{Q_\beta} S_\beta(E) f(Z+1, Q_\beta - E) dE}{\int_0^{Q_\beta} S_\beta(E) f(Z+1, Q_\beta - E) dE} \tag{2.2}$$

2.2 Kratz-Herrman Formula

The Kratz-Herrman Formula was first published in 1973 by K.-L. Kratz and G. Herrmann[19]. At that time there were only about 40 known precursors with measured half-lives and P_n. It was an improvement over a formula from Amiel and Feldstein where P_n was given as such:

$$P_n = a(Q_\beta - S_n)^m \tag{2.3}$$

Details of this approach can be found in the following reference [1], but the major issue is that P_n should not just depend on energy window $(Q_\beta - S_n)$. Going back to Equation 2.2, there is an introduction of a cut-off energy C below which S_β is assumed to be zero and

above which it is constant.

$$P_n = \frac{\int_{S_n}^{Q_\beta} S_\beta(E) f(Z+1, Q_\beta - E) dE}{\int_{C}^{Q_\beta} S_\beta(E) f(Z+1, Q_\beta - E) dE} \tag{2.4}$$

Where C is dependent upon nuclear mass of the precursor nucleus and is given as such:

$$\begin{aligned} C &= 0[MeV] && even - even, \\ C &= \frac{13}{\sqrt{A}}[MeV] && odd - mass, \\ C &= \frac{26}{\sqrt{A}}[MeV] && odd - odd \end{aligned} \tag{2.5}$$

Also the additional assumption for the Fermi integral can be stated as such:

$$f(Z+1, Q_\beta - E) \approx (Q_\beta - E)^5 \tag{2.6}$$

This leads to the following expression for P_n which is commonly referred to as the "Kratz-Hermann Formula":

$$P_n \simeq a\left(\frac{Q_\beta - S_n}{Q_\beta - C}\right)^b \tag{2.7}$$

Where a and b linear fit parameters based on a logP_n and log$(Q_\beta - S_n)/(Q_\beta - C)$ with experimental data for P_n. Q_β and S_n must be taken from a mass model, and in the case of KHF from Pfeiffer et. al the masses were taken from 1995 mass compilation by Audi and Wapstra and FRDM where no experimental values were found [28]. We cite this work since it is the most advanced calculations within KHF to date. While ENDF VI uses earlier KHF calculations, it would be best to compare a newer theory (EDM) with the most current KHF calculations. Also these calculations are the source of the ENDF/B-VII.0 delayed neutron calculations in 2006 [11].

Numerous advancements in experimental data were available in 2002 compared to the original work in 1973. Also, Pfeiffer et al. advanced a new determination for the linear fit parameters that uses 2 different values dependent upon the region within the nuclear chart. The historical values are given in the following table and then followed by the values used by Pfeiffer et al. These tables are reproduced from the Pfeiffer et al. reference [28].

Table 2.1: Parameters from fits to the Kratz-Herrmann-Formula from literature.

Reference	Parameters	
	a [%]	b
Kratz and Hermann (1973)	25	2.1 ± 0.2
Kratz and Hermann (1973)	51	3.6 ± 0.3
Mann (1984)	123.4	4.34
Mann (1984)	54 +31/-20	3.44 ± 0.51
England (1986)	44.08	4.119

Table 2.2: Parameters from fits to the Kratz-Herrmann-Formula in different mass regions in Pfeiffer et al.

Region	Lin. Regression			Least-squares fit		
	a [%]	b	r^2	a [%]	b	red. X^2
$29 \leq Z \leq 43$	88.23	4.11	0.81	105.76 ± 37.67	5.51 ± 0.61	80.97
$47 \leq Z \leq 57$	84.35	3.89	0.86	123.09 ± 41.17	4.68 ± 0.38	57.49
$29 \leq Z \leq 57$	85.16	3.99	0.83	80.58 ± 20.72	4.72 ± 0.34	78.23

The complete list of KHF values in the Pfeiffer tables are not reproduced here. The bibliography contains a link to the original paper and the data can be found there. While these are not the values used in ORIGEN, this is the largest advancement of KHF that will be compared alongside EDM and ORIGEN in the results. It should be noted that some advancements have been made over KHF using systematic arguments when including known half-life relations with P_n as is described in this reference [23], but these results are not reflected in any ENDF evaluation to date and it is not strictly a KHF theory. Later work should compare this theory as well. With the programs and codes developed in producing this work, this comparison would be easy to produce.

2.3 Effective Density Model

2.3.1 Introduction

The Effective Density Model is a phenomenological model for β-delayed neutron emission probability in similar fashion to the KHF. The critical difference here lies in the evaluation of the β-strength function. The assumption in EDM is that the statistical level density of a back-shifted Fermi-gas model is approximately S_β [2, 13].

$$S_\beta(E) \approx \rho(E) = \frac{exp(a_d\sqrt{E})}{E^{3/2}} \tag{2.8}$$

Substituting into Equation 2.2 we get the following expression for P_n:

$$P_n = \frac{\int_{S_n}^{Q_\beta} exp(a_d\sqrt{E})E^{-3/2}f(Z+1, Q_\beta - E)dE}{\int_0^{Q_\beta} exp(a_d\sqrt{E})E^{-3/2}f(Z+1, Q_\beta - E)dE} \tag{2.9}$$

Where the Fermi integral is taken from reference [40] (the normal approximation is not valid for high Z due to coulomb effects) and a_d is given as the total level density parameter to be about $\sqrt{A/8}$ [13]. However, this value needs to be adjusted since not all of the levels can participate in β-decay. This value is adjusted to experimental P_n data by the introduction of phenomenological parameter, a_d, and could be further tuned with new experimental data or by other constraints as discussed in Section 4.6. In the EDM, a_d is given phenomenologically such:

$$\begin{aligned} a_d(Z,N) &= a_1N' + a_2Z' + a_3\sqrt{N} + exp(m) \\ , N' &= N - (N_m^i + 2), \\ Z' &= Z - Z_m^i \end{aligned} \tag{2.10}$$

where N_m^i and Z_m^i are the last closed neutron and proton shells (28, 50, 82), and

$$m = \begin{cases} m_n/\sqrt{N} & N = N_m^i + 2, 3 \\ 0 & otherwise \end{cases} \tag{2.11}$$

The exact values for these parameters can be found in the reference paper. What is important to note is how it would compare to experiment where possible. This is shown in the following figure reproduced from Ref. [25]:

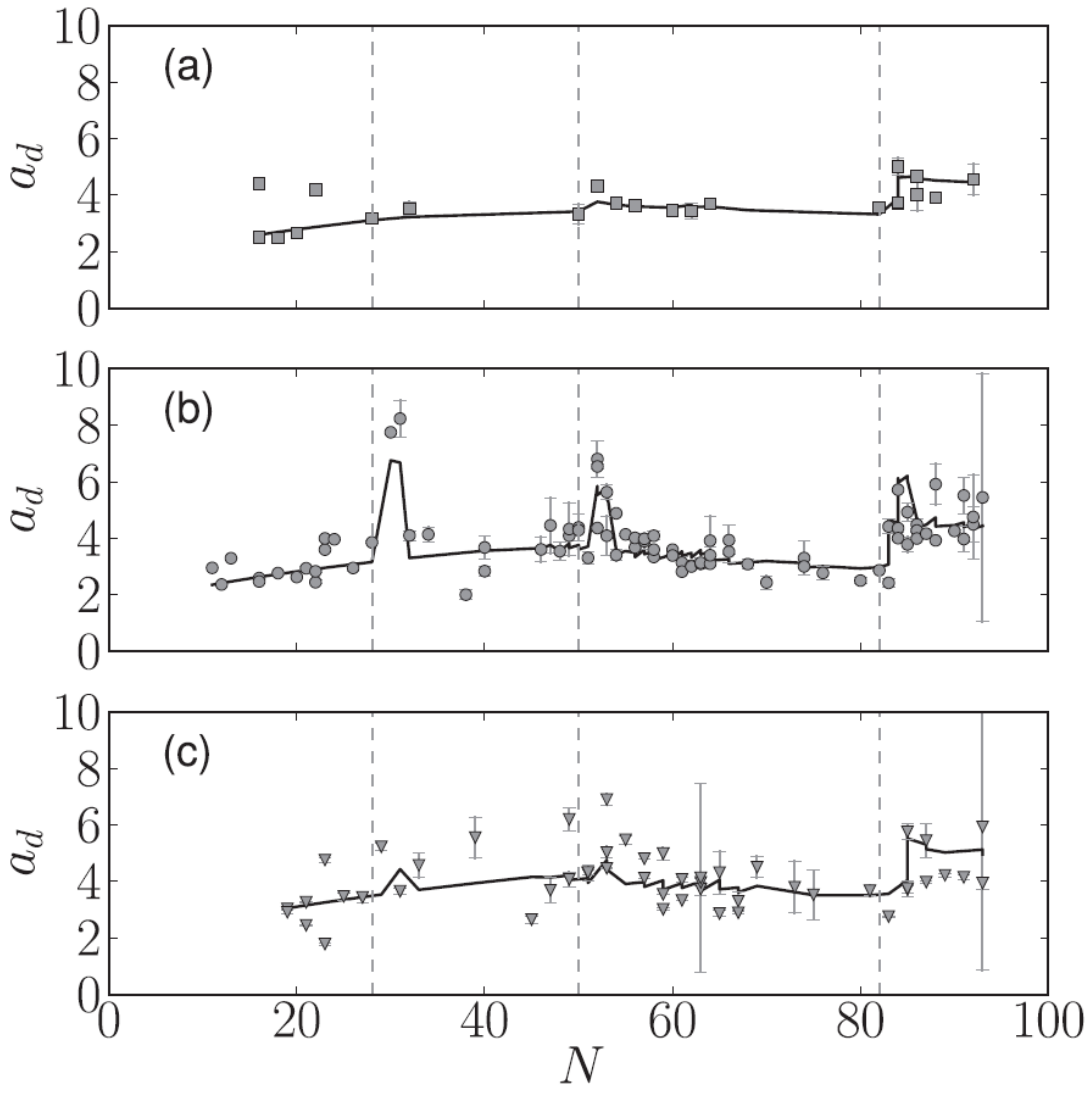

Figure 2.1: Effective density parameter determined from experimental data (points) and calculated from Eq. 2.10 (solid lines) as function of the number of neutrons N. The subplots present the (a) even-even, (b) odd-mass, and (c) odd-odd isotopes. The dashed lines show the magic numbers (28, 50, 82).

In the this reference, the experimental data set was based upon the Pfeiffer et al. data [28] and ENSDF where any new experimental data was available. Q_β and S_n are taken from the AME2012 atomic mass evaluation [36] (the most recent as of this work). a_d can thus be computed from experimental values P_n, Q_b, and S_n. Uncertainties shown above are propagated from the experimental values. It can be observed that near the shell gaps there is significant non-linear behavior. We suggest that in these places there could be significant improvements made by employing a more detailed and microscopic method such as the one described in this reference [5].

2.3.2 Comparing EDM to KHF

One insight that is given by Miernik is that when working out the effective density parameter for KHF it can be shown that KHF is effectively a low-order expansion of EDM. To show this, we see that S_β is modeled by KHF as a function of E^{-x} where $x \sim 0.5 - 1.5$ and observing that the leading order of the Taylor expansion for equation 2.8 is $E^{-3/2} and E^{-1}$. Recall that the value b is fitted to be around 4.5 to 5.5 from the KHF equation 2.7 and table 2.2. This difference between the first order expansion and higher order expansion thus lines up with the difference between KHF and EDM with the expected value of $b = 6$.

When comparing how this theory reproduces experimental results to other theories, a normalized χ^2 calculation is given in reference [25]:

Table 2.3: Normalized χ^2 (total χ^2 divided by the number of experimental points) calculated for Pn predictions of the theoretical models.

Model	Normalized χ^2
EDM	66
McCutchan[23]	78
KHF[23]	109
Gross theory[34]	415
QRPA[28]	548

For our purposes it is important to compare even further the differences between KHF and EDM. The 2013 EDM paper contains a few charts that help further emphasize the differences

between the results of predictions between these theories (See Figure 3 in Reference [25]). We have also provided figures that illustrates the difference in P_n across the entire chart of nuclides in the first subsection of the Results chapter.

2.3.3 Multiple Neutron Emission

It is in principle possible to emit multiple neutrons from a single precursor assuming that Q_β is above S_{xn} which corresponds to the xth neutron separation energy (e.g. 2 neutron separation energy (S_{2n})). In most nuclear engineering applications the probability of seeing neutrons from multiple delayed-neutron emissions is vanishingly small since the FPY for nuclei that have a higher probability of multiple neutron emission is usually orders of magnitude less than the most abundant nuclei. However, it is still possible that 2-neutron emission will contribute since the yields of those nuclei may still be significant. Above Iron there are three experimentally known cases of 2n emission: ^{86}Ga, $^{98,100}Rb$. The yields of these nuclei are on the order of $\leq 10^{-5}$, and P_{2n} is 20(10)%, .060(9)%, and 0.16(8)% respectively. Since there are so few verified cases it is important for theory to address this issue for nuclei that have higher yields. As mentioned before ENDF-B/VII.1 has multiple neutron emission data in File 8, but ORIGEN did not have the capability to include this data until recently.

The EDM can also be extended to multiple delayed neutron emission. It is assumed that the decays are sequential and not multi-body decays. For complete equations and details of this approach see the following reference [24]. Some of the EDM calculations that follow do not assume the multiple neutron decay and instead P_n is calculated to be the total as described in the above section. However, the capability to do calculations accounting for multiple neutron emission exists, and several cases were run.

We will move on to how these theories affect the calculations of isotopic concentrations and total delayed neutron emission in a few fission burst cases.

2.4 ORIGEN

2.4.1 Introduction

ORIGEN is the **O**ak **R**idge **I**sotope **Gen**eration code within a larger code package called SCALE that is used for nuclear engineering applications all over the globe. Some of those applications include: criticality safety, radiation shielding, cross-section processing, reactor physics, sensitivity and uncertainty analysis, and spent fuel and high-level waste characterization. ORIGEN explicitly deals with depletion and decay, irradiation, and decay heat. It primarily solves the following equation for the generation and depletion of any given nuclide over time (taken from the ORIGEN manual of SCALE 6.2):

$$\frac{dN_i}{dt} = \underbrace{\sum_{j=1}^{m} l_{ij}\lambda_j N_j}_{\text{decay to } N_i} + \underbrace{\Phi \sum_{k=1}^{m} f_{ik}\sigma_k N_k}_{\text{absorption to } N_i} - \underbrace{(\lambda_i + \Phi\sigma_i)N_i}_{\text{transmutation away from } N_i} \quad , \qquad i = 1, \ldots, m \tag{2.12}$$

where N_i is the atom density of nuclide i, λ_i is the radioactive disintegration constant of nuclide i, σ_i is the spectrum-averaged neutron absorption cross section of nuclide i, Φ is the space-energy-averaged neutron flux, l_{ij} is the branching fractions of radioactive disintegration from other nuclides j, f_{ik} is the branching fraction for neutron absorption by other nuclides k that lead to the formation of species i.

There are various solvers for this equation within the ORIGEN package, and for our purposes we are using the CRAM solver developed by Aarno Isotalo. This is a solver based on the Chebyshev Rational Approximation Method (CRAM) which is far more accurate than the other solvers ORIGEN has available. Details for this solver and the solution to the above equation can be found in the following reference: [30].

2.4.2 Neutron Sources and Decay Data in ORIGEN

Delayed neutrons that are acting as a source for fission are generally only important on the time scale of about ten seconds, but the exact profile of this source and which nuclides produce them is of great interest. Computational methods and neutron decay data in ORIGEN are adopted from SOURCES 4C, a code developed at Los Alamos [42]. In this code we are mostly concerned with the delayed neutron aspect which in SOURCES has 105 delayed neutron precursors with spectra. Since the calculations will be various fission bursts, we would also like to know just how many neutrons are emitted at specific times. The code above essentially follows the following formula for delayed neutron activity:

$$n_{delayed}(t) = \sum_{i=1}^{105} \lambda P_n^i Y_{indep}^i e^{-\lambda_i t} \tag{2.13}$$

Where Y_{indep} is the independent yield of the nuclide produced from fission. All other quantities are as they have been defined before. While the above is concerned with neutron generation from 105 precursors, there are least 271 important delayed neutron precursors [4]. When we later examine the delayed neutron sources we must keep this fact in mind. Updating the SOURCES 4C code to include all known data is a task that is outside of the scope of this current work and is for future studies.

What is possible is the manipulation of the decay libraries for individual nuclides. Thanks to the API [39], this task is both achievable and easy to test within a shorter time frame than redeveloping an entire library. The ORIGEN library is divided into three sub-libraries and we are most concerned with the fission products. A decay library contains a nuclide and some of its most relevant properties. Most of the data is taken from ENDF-B/VII.1 and as we know those predictions come from the Kawano and Möller calculations [16] and experimental data. We now have a very definable task: change the delayed neutron data and see the effects on neutron and isotope production with benchmark calculations.

The decay library specifically contains the following information that is important to our interests as described in ORIGENLIB documentation within the SCALE code package:

fission product yields, radioactive decay constants, branching ratios, recoverable decay energy values (Q_β), and fraction of energy due to photons. We will mostly focus on the branching ratios for this work, but those adjustments will have a direct effect on the FPYs even though it won't be possible to model this yet. That work will be done in collaboration with Marco Pigni and is expected to see some results within the year. The other data mentioned should be updated as well, and where it is possible to do this with new experimental data; however, calculations are not presented here since the comparisons are mostly concerned with EDM and ENDF-B/VII.1. This is left to future studies.

The specific work done on ORIGEN on my part is the development of codes to change the branching ratios of individual nuclei and produce new libraries that can be used for ORIGEN calculations. The branching ratios can be taken from any source in principle, but in this work the following are used: ENSDF, Pfeiffer and Möller calculations (a large update to the 2003 calculation is expected within the year), and the new Effective Density Model. These codes are a useful template for further modification of libraries as well as creation of new standard libraries for use within ORIGEN.

2.4.3 Calculations and Benchmarks

Calculations were run on the Jupiter cluster at ORNL with the SCALE 6.2beta4 and SCALE 6.3beta1 and the individual details for each calculation can be found in their respective files. A sample input deck and relevant output is produced in the Appendix C.1.

In order to compare the effects of changing P_n values, the results using default decay library was compared to three different cases: KHF, EDM, and EDM with experimental data (EDM-Exp). There were three different induced fission burst calculations: ^{238}U with fast neutrons, ^{235}U with 14 MeV neutrons, and ^{239}Pu with 14 MeV neutrons. In each case the calculation simulated all parameters to at least 24 hours with varying time steps. This leads to 12 different sets of data in all.

I developed a code to modify the decay library using the ORIGEN API [39]. This code reads in new data from EDM or KHF or any other theory with a given format, and then

changes the ORIGEN decay library accordingly. In our case it was substituting the new P_n values for each nuclide that both existed in the ORIGEN library and in the specified theory.

A list of experimentally obtained values from ENSDF can be applied as a filter so that theoretical values are only used for non-experimentally measured data. In this application, it was determined that ENDF/B-VII.I data files contain experimental data for 97 isotopes which had their P_n values given from ENSDF or 2002PF04. This value is not in agreement with the most recent experimental measurements. While there exists 163 experimental P_n values as of late 2013 [25], the calculations in this work are compared with the latest version used by ORIGEN. It is noted that it would also not take much time to run a calculation with all of this new experimental data since the code can now be adapted to include almost any decay data desired.

Additionally, the isotopic concentrations can be compared, there was a selection criteria that limited the set of isotopes analyzed to those that are relevant for fallout. The list can be found in the Appendix C. For the delayed neutron sources, we identify the contributors with the largest changes and also list the total percent contribution to the neutrons produced at each time step.

Various analytical tools were employed or developed so that the ORIGEN outputs could be read more easily or visualized. One of the most important tools is the visualization of changes on a chart of nuclides. This helps the reader quickly see the regions of greatest change for any given output data. Such charts can be seen in the Results section.

Table of breakdown of default libraries and comparisons shown in the Results chapter 3:

Table 2.4: Table of Calculations Represented in this Work

Calculation	P_n **Source**
ORIGEN	ENDF/B VII.1 + QRPA Hauser-Feshbach
ORIGEN + EDM	EDM
ORIGEN + KHF	KHF
ORIGEN + EDM + EXP	ENSDF + EDM

2.5 Verification of Data in ENDF

Many times it has been said that the state of Nuclear data is not great, but quantifying just what that means can sometimes be problematic. In this work several issues were identified and a partial list of nuclides that have values of P_n in ENDF VII.1B that vary from the literature were identified. The differences between ENDF-B/VII.I values and experimental data became clear when only 97 values were identified in ENDF as having a source from ENSDF or 2002PF04. Miernik identifies at least 163 experimental values and 2002PF04 gives 128 values. The ENDF File 8 data was supposedly evaluated in August of 2011, yet it cites fewer experimental values than a paper that predates it by more than 8 years. One possible reason for the discrepancy is that many have argued that a few of the data is unreliable, and this can be seen clearly for one such case in the appendix B.1. Rudstam presents an analysis in his compilation in 1993 of some of the data and the reliability of particular measurements [32]. While one can argue about what exact data should be used and if certain experiments should be discounted, there needs to be more experiments on data that is doubted. It appears that such a discrepancies are being resolved by theory, and as can be seen, different theories will yield different results. This work hopes to motivate specific updates in the decay data for ENDF-B/VII.1 by listing the nuclides that have experimental data, but are still for some reason calculated via QRPA Hauser-Feshbach. The effect of updating a few of these P_n values to recent experimental values for the calculation of the total delayed neutron fraction is explored in the results section.

It is also known that there are large differences between the cumulative yields of some nuclei. In a paper by Katakura et al. [15], three nuclei: ^{86}Ge, ^{88}As, and ^{100}Rb were identified has having yields that appear to be too large. In these cases the difference between the reported yield by ENDF and what should be expected with a proper charge-mass distribution is orders of magnitude different. Since each of these nuclides undergo beta-delayed neutron emission, this will have a direct effect on the production of isotopes and the total delayed neutron fraction. The exact effect of the yield change on the production of isotopes was not studied in this work due to ORIGEN not supporting a current way to change the yields

consistently. In spite of being unable to treat the cumulative yields consistently, one can get a good idea of just how much the delayed neutron fraction will change and the feeding rates to other isotopes simply by multiplying the appropriate decay channel branching ratio by the cumulative yield. To this extent, the effect of changing these yields is shown in the results.

2.6 Microscopic Methods

This section will summarize the calculations done by Kawano and Möller that are contained in the ENDF/B-VII.1 evaluation. The main reference paper is from 2008: [16]. However, the combination of a microscopic-macroscopic theory with QRPA has been done for many years and is the other theory contained within the Kratz-Möller paper on KHF that was the basis of the ENDF/B-VII.0 beta-decay data [6, 28]. Earlier models within this vein are described in detail within the following references: [20, 26]. The basic random phase approximation and Hartree-Fock-Bogoliubov theory is also described within the well known text: The Nuclear Many-Body Problem by Ring and Schuck [31]. Reproducing more of this theory here is not the focus of this work.

2.6.1 FRDM-QRPA and Hauser-Feshbach

QRPA is a method for calculating decay matrix elements between the initial and final states of nuclei (in our case: beta-decay). While different models chose to calculate the rates from one state to another in many ways, QRPA requires some inputs such as nuclear wave functions and single-particle energies which can also be calculated within a given potential with the possible residual interactions. For the model in ENDF, FRDM is used for these inputs. FRDM essentially serves as the framework for QRPA calculations by giving energy levels for Q_β, S_n, and other quantities of interest like the ground-states of various nuclei. FRDM been mentioned a number of times already and is more fully described within the

attachment, so we will not focus on it. Using this information, QRPA is used to calculate the branching ratios from a given initial state to a given final state.

Hauser-Feshbach is a statistical model for calculating the transmission coefficients of all final states to a compound state. The excited states from QRPA are assumed to be a compound state. The Hauser-Feshbach theory is described fully in the seminal paper: [14]. This theory is then used within the CGM code developed out at LANL to provide the final calculations of spectra for gamma decay and neutron emission. For decays above $S_{xn}; x \geq 2$, sequential multiple neutron emission is possible. This means that this is a microscopic method for decay, but it is not an entirely microscopic method since it relies upon FRDM for many inputs. Also, this method was only used in ENDF when insufficient ENSDF data was available.

The schematic description of the GCM code and further description of the Hauser-Feshbach model is given here: [16, 18]. This work will not expound upon it any further. Since this calculation is the basis for ENDF/B-VII.1 when there is no experimental data, we will for the most part now be referring to this simply as the ENDF calculations and default library for ORIGEN in the following Results chapter.

Chapter 3

Results

In comparing the models of ORIGEN, KHF, and EDM, we begin by comparing the P_n values of each model to one another and to the default library of ORIGEN, ENDF/B-VII.1. The next focus will be on the changes to isotope concentrations due to these different models. Then the calculations concerning delayed neutron emission will be presented. Finally the results that compare the effect of yields, new experimental P_n values, and delayed neutron fractions will be presented.

3.1 Differences of P_n in ORIGEN, KHF, and EDM

Each of the figures below provide a graphical representation of a specific library across the nuclear chart. Figures 3.1 through 3.3 show the P_n on a log scale. Some things of note: Black squares represent no possibility of neutron emission, but are included for comparison to other models in which a neutron emission branching ratio is given. No nuclei that are not found in ORIGEN have been added. These nuclei might undergo single- and multiple-neutron emission, but there is no appreciable yield for these nuclei as can be seen in Figure 1.1 and 1.2. As such those nuclei are ignored in all the following calculations. It is also worth mentioning that within ORIGEN, if there is a possibility of multiple neutron emission with

in ENDF/B-VII.1, any values given for multiple neutron emission are simply added to that of P_n. This can be represented as follows:

$$P_n = \sum_{x=1}^{4} P_{xn} \tag{3.1}$$

The possibility of three and four neutron emission becomes vanishingly small for most nuclei, but is included in the QRPA Hauser-Feshbach models nonetheless. Since ORIGEN is not exactly using the ENDF-B/VII.1 data, we will talk about the default ORIGEN library simply as the ORIGEN library.

The figures 3.4 through 3.7 give a comparison between these different P_n values by implementing a absolute percent change followed by a graphic that details weather that change is positive or negative with respect to ORIGEN. The equation solved for each isotope is given as such:

$$Absolute \quad \% \quad Change = \left| \frac{P_n(ORIGEN) - P_n(EDM)}{P_n(ORIGEN)} \right| * 100\% \tag{3.2}$$

When P_n does not exist for ORIGEN the value becomes undefined and as such the black boxes simply represent where there was no previous data for ORIGEN.

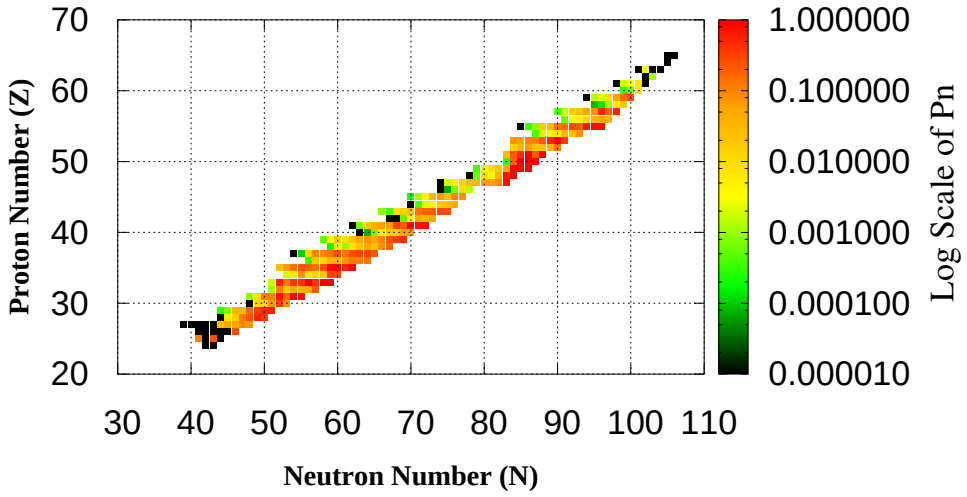

Figure 3.1: P_n given by ORIGEN

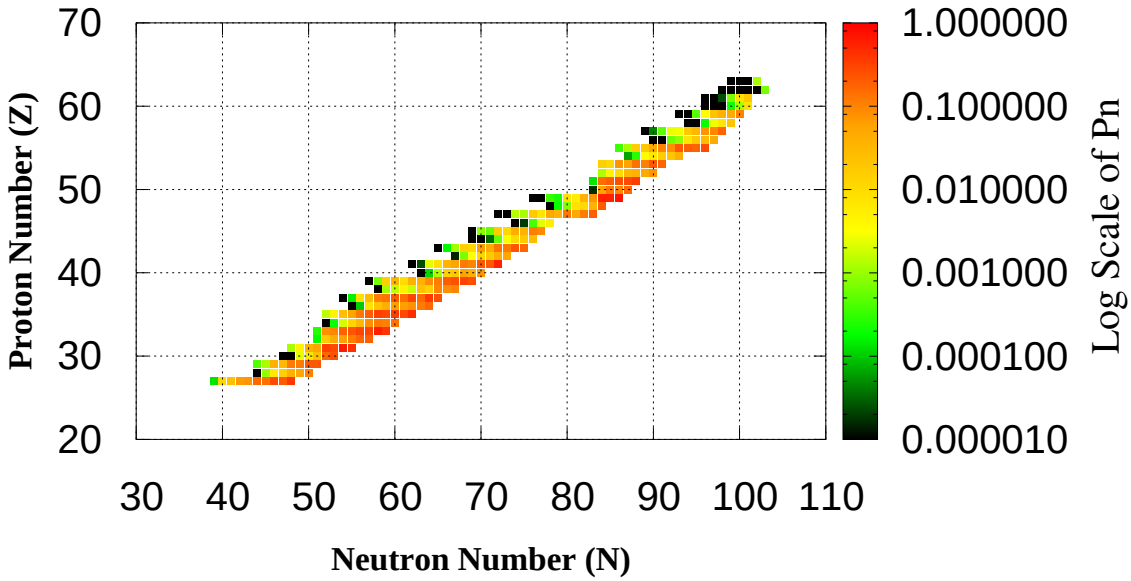

Figure 3.2: P_n given by KHF

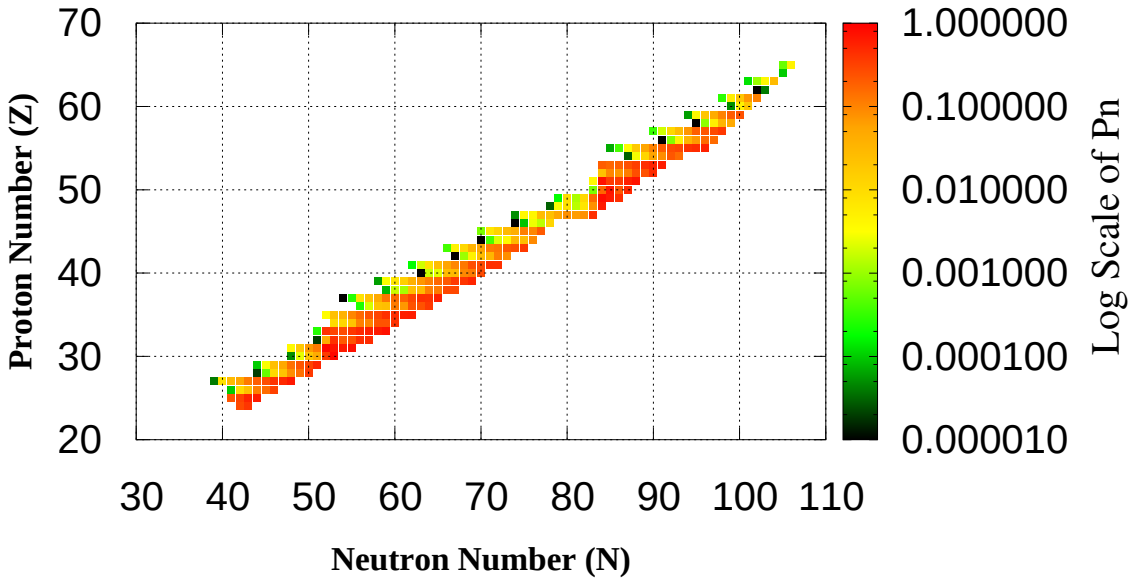

Figure 3.3: Total P_n given by EDM

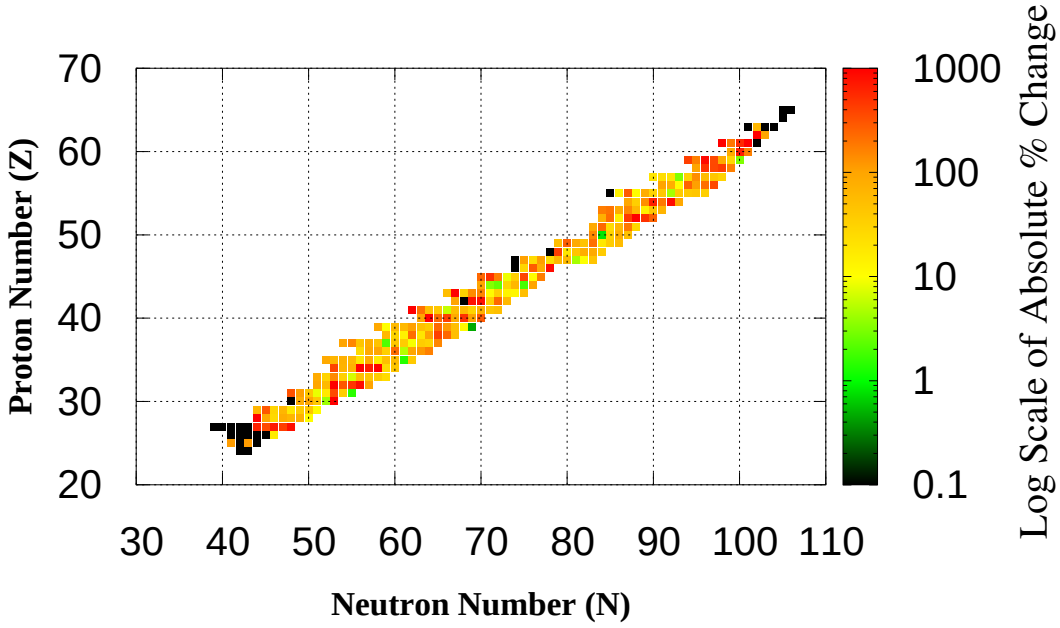

Figure 3.4: Absolute Percent Change in P_n from ORIGEN to EDM.

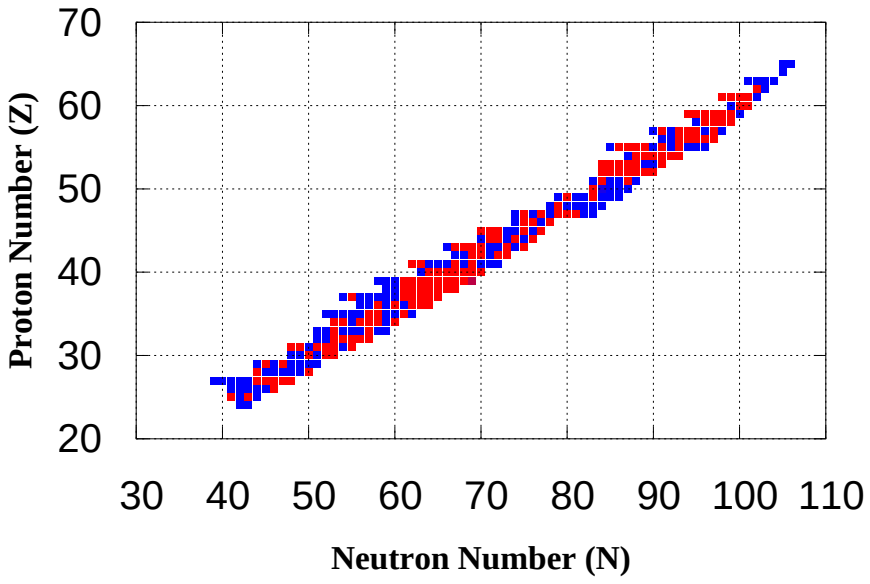

Figure 3.5: Blue represents lower values of P_n in EDM (wrt. ORIGEN). Red represents higher values.

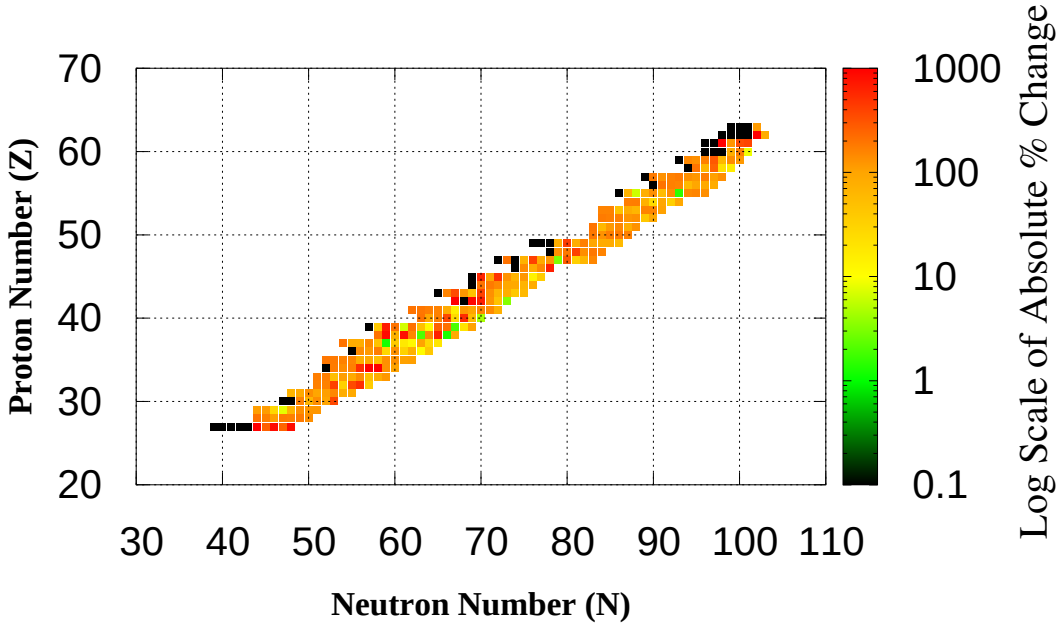

Figure 3.6: Absolute Percent Change in P_n from ORIGEN to KHF.

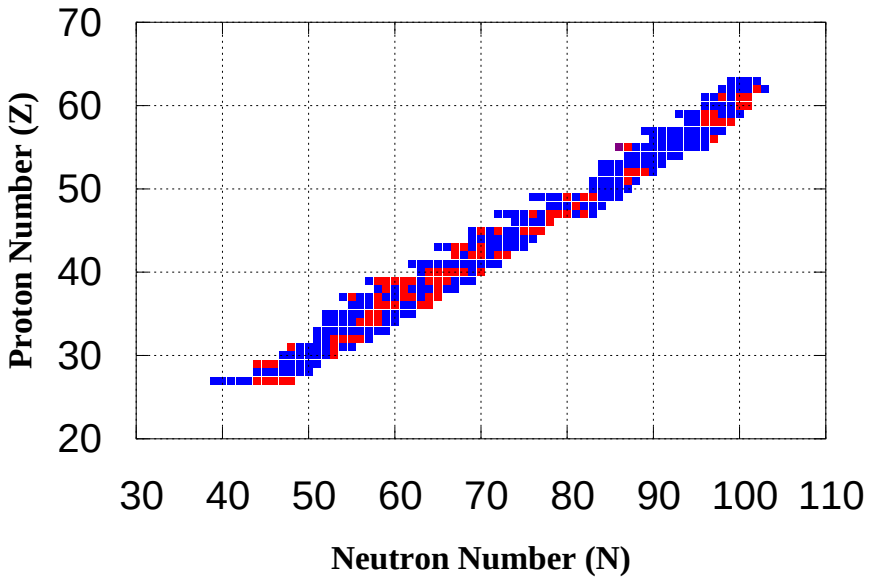

Figure 3.7: Blue represents lower values in KHF (wrt. ORIGEN). Red represents higher values.

3.2 Isotopic Concentration Calculations with Varying Bursts

Using ORIGEN with the setup described in section 2.4.3, we were able to produce many outputs that will be examined in detail for the changes to the abundance of particular nuclei listed in the Appendix C.

All calculations were done in comparison with the default ORIGEN library (ENDF/B-VII.I) which is described in detail in the ORIGENLIB documentation of SCALE 6.2. We will show at least three tables for each of the theories compared that contain all nuclides that had changes of greater than 1% in their concentration as well as initial concentrations of greater than $1 * 10^{-10}$. In some cases, the fallout selection criteria is omitted to show changes in areas that lie on the boundaries of our region of interest. For instance table 3.7 shows an extreme increase in the production of ^{65}Cu.

3.2.1 ^{235}U Fission Burst with Fast Neutrons

Table 3.1: ^{235}U fast neutron burst. Conc. A is the isotopic concentration in gram-atoms using ENDF/B-VII.I. Conc. B is using EDM. Concentrations given 24 hours after burst.

Z	A	Conc. A	Conc. B	$\|A - B\|$	Diff. [%]
Br	84	1.86E-09	1.80E-09	6.13E-11	-3.30E+00
Y	93	7.21E+03	7.05E+03	1.55E+02	-2.15E+00
I	134	4.44E-03	4.52E-03	8.64E-05	1.95E+00
Rb	88	9.53E+00	9.35E+00	1.82E-01	-1.91E+00
Kr	88	8.19E+01	8.03E+01	1.57E+00	-1.91E+00
I	135	3.12E+03	3.06E+03	5.75E+01	-1.85E+00
Xe^m	135	2.08E+01	2.04E+01	3.83E-01	-1.85E+00
Xe	135	1.06E+04	1.04E+04	1.89E+02	-1.78E+00
Cs	138	7.12E-08	6.99E-08	1.21E-09	-1.70E+00
Kr	87	8.19E-02	8.05E-02	1.37E-03	-1.67E+00

Table 3.2: ^{235}U fast neutron burst. Conc. A is the isotopic concentration in gram-atoms using ENDF/B-VII.I. Conc. B is using KHF. Concentrations given 24 hours after burst.

Z	A	Conc. A	Conc. B	$\lvert A - B \rvert$	Diff. [%]
Br	84	1.86E-09	1.67E-09	1.89E-10	-1.02E+01
Kr	87	8.19E-02	7.95E-02	2.38E-03	-2.91E+00
Y	94	1.92E-17	1.97E-17	5.19E-19	2.70E+00
Y^m	93	5.77E-53	5.65E-53	1.23E-54	-2.13E+00
Y	93	7.21E+03	7.06E+03	1.49E+02	-2.06E+00
Rb	88	9.53E+00	9.43E+00	1.08E-01	-1.13E+00
Kr	88	8.19E+01	8.09E+01	9.29E-01	-1.13E+00

Table 3.3: ^{235}U fast neutron burst. Conc. A is the isotopic concentration in gram-atoms using ENDF/B-VII.I. Conc. B is using EDM + ENDF/B experimental data. Concentrations given 24 hours after burst.

Z	A	Conc. A	Conc. B	$\lvert A - B \rvert$	Diff. [%]
Tc^m	99	1.91E+03	1.92E+03	9.42E+00	4.94E-01
Tc	99	4.34E+03	4.37E+03	2.14E+01	4.94E-01
Mo	99	2.41E+04	2.42E+04	1.19E+02	4.93E-01

3.2.2 ^{238}U Fission Burst with Fast Neutrons

The exact ORIGEN input deck for this calculation can be found in the Appendix C.1.

Table 3.4: ^{238}U fast neutron burst. Conc. A is the isotopic concentration in gram-atoms using ENDF/B-VII.I. Conc. B is using EDM. Concentrations given 24 hours after burst.

Z	A	Conc. A	Conc. B	$\|A - B\|$	Diff. [%]
I	134	5.09E-07	5.48E-07	3.95E-08	7.76
Rb	88	6.29E-04	5.82E-04	4.69E-05	-7.46
Kr	88	5.40E-03	5.00E-03	4.02E-04	-7.46
I	135	3.79E-01	3.52E-01	2.75E-02	-7.25
Xe^m	135	2.53E-03	2.34E-03	1.83E-04	-7.25
Y	93	6.26E-01	5.98E-01	2.78E-02	-4.43
Ba	140	3.08E+00	3.03E+00	5.29E-02	-1.72
La	140	1.31E-01	1.29E-01	2.24E-03	-1.71
Y	92	1.02E-01	1.00E-01	1.71E-03	-1.68
Kr	87	5.81E-06	5.72E-06	9.42E-08	-1.62
Pr	144	1.06E-04	1.04E-04	1.71E-06	-1.62
Ce	144	2.51E+00	2.47E+00	4.06E-02	-1.62
Pr^m	144	4.21E-07	4.14E-07	6.81E-09	-1.62
Y^m	91	2.60E-02	2.63E-02	3.47E-04	1.33
Sr	91	4.69E-01	4.75E-01	6.26E-03	1.33
Y	91	1.77E+00	1.80E+00	2.37E-02	1.33
Zr	95	2.87E+00	2.91E+00	3.75E-02	1.30
Nb	95	2.78E-02	2.82E-02	3.62E-04	1.30
Nb^m	95	2.81E-04	2.85E-04	3.66E-06	1.30
Tc^m	99	2.19E-01	2.21E-01	2.42E-03	1.11
Tc	99	4.98E-01	5.03E-01	5.51E-03	1.11
Mo	99	2.76E+00	2.79E+00	3.05E-02	1.11
Ba	139	5.94E-05	5.88E-05	6.03E-07	-1.02

Table 3.5: ^{238}U fast neutron burst. Conc. A is the isotopic concentration in gram-atoms using ENDF/B-VII.I. Conc. B is using KHF. Concentrations given 24 hours after burst.

Z	A	Conc. A	Conc. B	$\lvert A - B \rvert$	Diff. [%]
Rb	88	6.29E-04	5.85E-04	4.38E-05	-6.97
Kr	88	5.40E-03	5.02E-03	3.77E-04	-6.97
Y	93	6.26E-01	5.99E-01	2.71E-02	-4.34
Kr	87	5.81E-06	5.65E-06	1.62E-07	-2.79
Y^m	91	2.60E-02	2.65E-02	4.74E-04	1.83
Sr	91	4.69E-01	4.78E-01	8.57E-03	1.83
Y	91	1.77E+00	1.81E+00	3.24E-02	1.83
Tc	99	4.98E-01	4.91E-01	6.70E-03	-1.35
Tc^m	99	2.19E-01	2.16E-01	2.94E-03	-1.35
Y	92	1.02E-01	1.01E-01	1.16E-03	-1.13

Table 3.6: ^{238}U fast neutron burst. Conc. A is the isotopic concentration in gram-atoms using ENDF/B-VII.I. Conc. B is using EDM + ENDF/B-VII.I experimental data. Concentrations given 24 hours after burst.

Z	A	Conc. A	Conc. B	$\lvert A - B \rvert$	Diff. [%]
Tc^m	99	2.19E-01	2.21E-01	2.26E-03	1.03
Tc	99	4.98E-01	5.03E-01	5.13E-03	1.03

If one were to remove the restriction of the fallout nuclides and simply look for the largest changes when EDM is introduced to only non-experimental values, this would be the list of nuclides meeting the selection criteria.

Table 3.7: ^{238}U fast neutron burst. Conc. A is the isotopic concentration in gram-atoms using ENDF/B-VII.I. Conc. B is using EDM + ENDF/B-VII.I experimental data. Fallout selection criteria omitted. Concentrations given 24 hours after burst.

Z	A	Conc. A	Conc. B	$\lvert A - B \rvert$	Diff. [%]
Cu	65	2.28E-08	4.82E-08	2.54E-08	112
Kr^m	85	1.46E-02	1.53E-02	7.05E-04	4.85
Rb	85	3.28E-01	3.44E-01	1.59E-02	4.85
Kr	85	9.04E-02	9.47E-02	4.37E-03	4.83
Kr	86	7.50E-01	7.23E-01	2.74E-02	-3.66
Cu	66	7.21E-09	7.40E-09	1.87E-10	2.59
Ni	66	4.61E-06	4.73E-06	1.19E-07	2.59
Zn	66	1.48E-06	1.52E-06	3.82E-08	2.58
Cu	67	1.44E-05	1.47E-05	3.16E-07	2.19
Zn	67	4.03E-06	4.12E-06	8.82E-08	2.19
Ga	69	4.53E-05	4.59E-05	5.54E-07	1.22
Zn	68	3.04E-05	3.08E-05	3.42E-07	1.12
Tc^m	99	2.19E-01	2.21E-01	2.26E-03	1.03
Ru	99	1.52E-05	1.54E-05	1.57E-07	1.03
Tc	99	4.98E-01	5.03E-01	5.13E-03	1.03
Mo	99	2.76E+00	2.79E+00	2.85E-02	1.03

3.2.3 ^{235}U Fission Burst with 14 MeV Neutrons

Table 3.8: ^{235}U 14 MeV neutron burst. Conc. A is the isotopic concentration in gram-atoms using ENDF/B-VII.I. Conc. B is using EDM. Concentrations given 24 hours after burst.

Z	A	Conc. A	Conc. B	$\|A - B\|$	Diff. [%]
Y	93	2.44E-03	2.40E-03	4.58E-05	-1.87E+00
Kr	87	1.22E-08	1.20E-08	2.15E-10	-1.76E+00
Rb	88	2.59E-06	2.55E-06	4.33E-08	-1.67E+00
Kr	88	2.23E-05	2.19E-05	3.72E-07	-1.67E+00

Table 3.9: ^{235}U 14 MeV neutron burst. Conc. A is the isotopic concentration in gram-atoms using ENDF/B-VII.I. Conc. B is using KHF. Concentrations given 24 hours after burst.

Z	A	Conc. A	Conc. B	$\|A - B\|$	Diff. [%]
Kr	87	1.22E-08	1.19E-08	3.60E-10	-2.95E+00
Y	93	2.44E-03	2.40E-03	4.35E-05	-1.78E+00
Rb	88	2.59E-06	2.57E-06	2.49E-08	-9.60E-01
Kr	88	2.23E-05	2.21E-05	2.14E-07	-9.60E-01

There were no significant differences in concentrations for when replacing the ORIGEN library with EDM values only for values that ENDF/B-V.II does not have ENSDF experimental data for in it's database. The following table represents the changes to the only nuclides that had any significant change although none of them are in the fallout list.

Table 3.10: ^{235}U 14 MeV neutron burst. Conc. A is the isotopic concentration in gram-atoms using ENDF/B-VII.I. Conc. B is using EDM + ENDF/B-VII.I experimental data. Concentrations given 24 hours after burst. Fallout selection criteria omitted.

Z	A	Conc. A	Conc. B	$\|A - B\|$	Diff. [%]
Cu	65	3.25E-09	5.76E-09	2.52E-09	7.76E+01
Cu	67	1.11E-06	1.12E-06	1.67E-08	1.51E+00
Zn	67	3.41E-07	3.47E-07	5.15E-09	1.51E+00
Ni	66	5.05E-07	5.12E-07	6.84E-09	1.35E+00
Zn	66	1.81E-07	1.83E-07	2.42E-09	1.34E+00
Ga	69	3.16E-06	3.20E-06	3.97E-08	1.26E+00

3.2.4 ^{239}Pu Fission Burst with 14MeV Neutrons

Table 3.11: ^{239}Pu 14 MeV neutron burst. Conc. A is the isotopic concentration in gram-atoms using ENDF/B-VII.I. Conc. B is using EDM. Concentrations given 24 hours after burst.

Z	A	Conc. A	Conc. B	$\|A-B\|$	Diff. [%]
Y	93	1.52E-03	1.49E-03	2.07E-05	-1.36E+00
Kr	87	6.45E-09	6.38E-09	7.57E-11	-1.17E+00

Table 3.12: ^{239}Pu 14 MeV neutron burst. Conc. A is the isotopic concentration in gram-atoms using ENDF/B-VII.I. Conc. B is using KHF. Concentrations given 24 hours after burst.

Z	A	Conc. A	Conc. B	$\|A-B\|$	Diff. [%]
Y	93	4.29E-07	4.23E-07	5.55E-09	-1.29E+00

There were no significant differences in concentrations for when replacing the ORIGEN library with EDM values only for values that ENDF/B-V.II does not have ENSDF experimental data for in it's database. The following table represents the changes to the only nuclides that had any significant change although none of them are in the fallout list.

Table 3.13: ^{239}Pu 14 MeV neutron burst. Conc. A is the isotopic concentration in gram-atoms using ENDF/B-VII.I. Conc. B is using EDM + ENDF/B-VII.I experimental data. Concentrations given 24 hours after burst. Fallout selection criteria omitted.

Z	A	Conc. A	Conc. B	$\|A-B\|$	Diff. [%]
Cu	67	1.79E-07	1.83E-07	3.54E-09	1.98E+00
Zn	67	5.54E-08	5.65E-08	1.09E-09	1.97E+00

3.3 Multiple Neutron Emission with EDM

In this section, we compare the ORIGEN calculations done taking into account up to 2 neutron emission within the EDM framework. In the latest version of ENDF this data is also available from the QRPA Hauser-Feshbach model, but as mentioned above ORIGEN

did not treat it as a separate case. This section focuses on the explicit representation of sequential double neutron emission and the affects on calculations of isotope concentrations using the same cases and selection criteria as above. We only reproduce the ^{238}U fission burst with fast neutrons here since the changes in the other bursts follow the same patterns as those above.

3.3.1 ^{238}U Fission Burst with Fast Neutrons with Multiple Neutron Emission EDM

Table 3.14: ^{238}U fast neutron burst. Conc. A is the isotopic concentration in gram-atoms using ENDF/B-VII.I. Conc. B is using EDM with two neutron emission. Concentrations given 24 hours after burst.

Z	A	Conc. A	Conc. B	$\lvert A - B \rvert$	Diff. [%]
I	134	5.09E-07	5.49E-07	4.00E-08	7.87E+00
I	135	3.79E-01	3.52E-01	2.70E-02	-7.10E+00
Xe^m	135	2.53E-03	2.35E-03	1.80E-04	-7.10E+00
Rb	88	6.29E-04	5.89E-04	3.98E-05	-6.34E+00
Kr	88	5.40E-03	5.06E-03	3.42E-04	-6.34E+00
Y	93	6.26E-01	5.98E-01	2.80E-02	-4.47E+00
Ba	139	5.94E-05	5.83E-05	1.06E-06	-1.78E+00
Ba	140	3.08E+00	3.03E+00	4.98E-02	-1.62E+00
La	140	1.31E-01	1.29E-01	2.11E-03	-1.61E+00
Pr	144	1.06E-04	1.04E-04	1.63E-06	-1.54E+00
Ce	144	2.51E+00	2.47E+00	3.88E-02	-1.54E+00
Pr^m	144	4.21E-07	4.14E-07	6.50E-09	-1.54E+00
Kr	87	5.81E-06	5.73E-06	8.53E-08	-1.47E+00
Y	92	1.02E-01	1.01E-01	1.29E-03	-1.27E+00
Tc^m	99	2.19E-01	2.21E-01	2.33E-03	1.06E+00
Tc	99	4.98E-01	5.03E-01	5.30E-03	1.06E+00
Mo	99	2.76E+00	2.79E+00	2.94E-02	1.06E+00

Table 3.15: ^{238}U 14 MeV neutron burst. Conc. A is the isotopic concentration in gram-atoms using ENDF/B-VII.I. Conc. B is using EDM with two neutron emission + ENDF/B-VII.I experimental data. Concentrations given 24 hours after burst.

Z	A	Conc. A	Conc. B	$\|A - B\|$	Diff. [%]
Tc^m	99	2.19E-01	2.21E-01	2.08E-03	9.52E-01
Tc	99	4.98E-01	5.03E-01	4.74E-03	9.52E-01

Table 3.16: ^{238}U 14 MeV neutron burst. Conc. A is the isotopic concentration in gram-atoms using ENDF/B-VII.I. Conc. B is using EDM with two neutron emission + ENDF/B-VII.I experimental data. Concentrations given 24 hours after burst. Fallout selection criteria omitted.

Z	A	Conc. A	Conc. B	$\|A - B\|$	Diff. [%]
Cu	65	2.28E-08	5.05E-08	2.78E-08	1.22E+02
Kr	85	1.46E-02	1.53E-02	7.47E-04	5.13E+00
Rb	85	3.28E-01	3.45E-01	1.69E-02	5.13E+00
Kr	85	9.04E-02	9.50E-02	4.62E-03	5.12E+00
Kr	86	7.50E-01	7.23E-01	2.74E-02	-3.65E+00
Cu	66	7.21E-09	7.46E-09	2.46E-10	3.40E+00
Ni	66	4.61E-06	4.77E-06	1.57E-07	3.40E+00
Zn	66	1.48E-06	1.53E-06	5.03E-08	3.39E+00
Cu	67	1.44E-05	1.48E-05	3.45E-07	2.39E+00
Zn	67	4.03E-06	4.13E-06	9.63E-08	2.39E+00
Zn	68	3.04E-05	3.09E-05	4.97E-07	1.63E+00

3.4 Delayed Neutron Sources after Fission Bursts

SOURCES4C developed at LANL tracks 105 delayed neutron precursors that have delayed neutron spectra. They are listed below (adapted from the ORIGENLIB manual):

^{79}Zn	^{89}Br	^{97}Y	^{128}In	^{141}I
^{79}Ga	^{90}Br	^{97m}Y	^{129}In	^{142}I
^{80}Ga	^{91}Br	^{98}Y	^{129m}In	^{143}I
^{81}Ga	^{92}Br	^{98m}Y	^{130}In	^{141}Xe
^{82}Ga	^{93}Br	^{99}Y	^{131}In	^{142}Xe
^{83}Ga	^{92}Kr	^{100}Y	^{132}In	^{143}Xe
^{83}Ge	^{93}Kr	^{104}Zr	^{133}Sn	^{144}Xe
^{84}Ge	^{94}Kr	^{105}Zr	^{134}Sn	^{141}Cs
^{85}Ge	^{95}Kr	^{103}Nb	^{135}Sn	^{142}Cs
^{86}Ge	^{92}Rb	^{104}Nb	^{134m}Sb	^{143}Cs
^{84}As	^{93}Rb	^{105}Nb	^{135}Sb	^{144}Cs
^{85}As	^{94}Rb	^{106}Nb	^{136}Sb	^{145}Cs
^{86}As	^{95}Rb	^{109}Mo	^{137}Sb	^{146}Cs
^{87}As	^{96}Rb	^{110}Mo	^{136}Te	^{147}Cs
^{87}Se	^{97}Rb	^{109}Tc	^{137}Te	^{147}Ba
^{88}Se	^{98}Rb	^{110}Tc	^{138}Te	^{148}Ba
^{89}Se	^{99}Rb	^{122}Ag	^{139}Te	^{149}Ba
^{90}Se	^{97}Sr	^{123}Ag	^{137}I	^{150}Ba
^{91}Se	^{98}Sr	^{128}Cd	^{138}I	^{147}La
^{87}Br	^{99}Sr	^{127}In	^{139}I	^{149}La
^{88}Br	^{100}Sr	^{127m}In	^{140}I	^{150}La

The following figures represent the neutrons emitted by the 105 tracked precursors above. It is worth noting that due to limitations within ORIGEN and SOURCES4C that the capability of tracking all 271 delayed precursors from the Brady thesis has not yet been implemented. All data that follows below has that restriction on it and should not be taken as results for all delayed neutron precursors. Additionally since the yields are not consistent with these models that are being introduced, a more thorough study is proposed within the conclusions. The models represented below also only consider single neutron emission

so as not to bring in even larger inconsistencies with the current capabilities of SOURCES utilized by ORIGEN. This is done since SOURCES does not have methods for computations surrounding multiple neutron emission.

The figures in the next section, represent the delayed neutron emitters that produce the largest number of neutrons after a few seconds. They were then tracked for 6 minutes since after a few minutes only nuclides in group 1 and 2 have significant contribution. Since SOURCES also includes the spectra for these decay, the neutron energy over time could be tracked, but was not in this work. It is worth noting that most of the emitters that are not being tracked in these graphics still have a significant contribution at short time scales, and those nuclides are of specific concern in addressing the gap between delayed neutron yield produced in simulations and experimental data. Also a great majority of the remaining 166 delayed neutron precursors in Brady's analysis that are not present here are short lived isotopes. The full investigation of that data will take place at a later time.

3.4.1 ^{238}U Fission Burst with Fast Neutrons

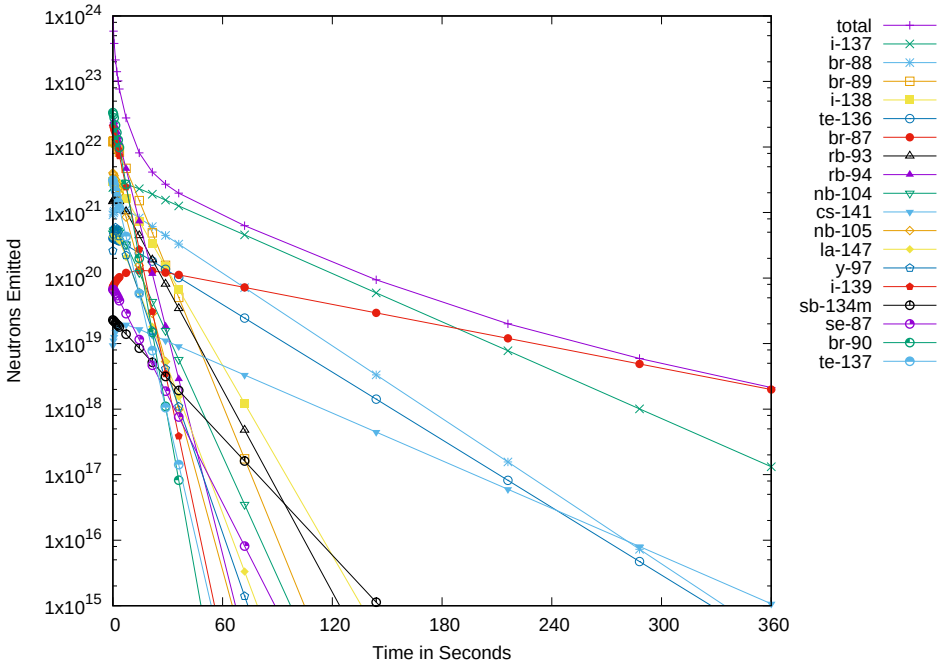

Figure 3.8: Top 20 Delayed Neutron Emitters for 6 Minutes after ^{238}U Burst with ORIGEN

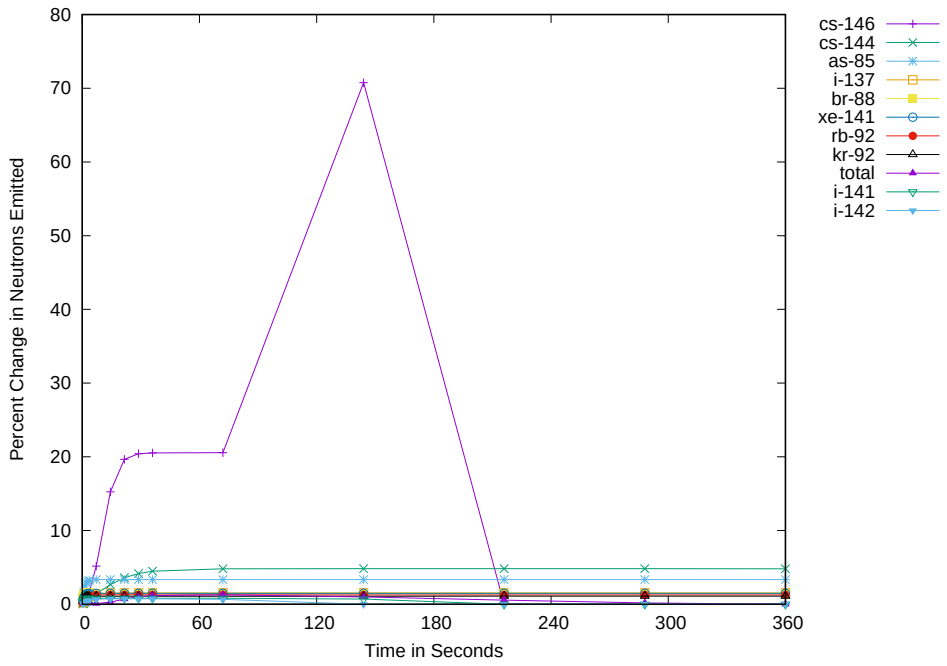

Figure 3.9: Delayed Neutron Emitters with more than 1% Change at 1 Minute with EDM (wrt. ORIGEN)

Since ^{146}Cs has a such a large difference in its emission of neutrons, we remove it so that it is easier to see what isotopes are changing the most. Each of the isotopes can have their group identified in the table provided in the appendix.

It is also important to visualize the 105 delayed neutron precursors within the context of groups. Each of the 105 isotopes have been binned into 6 groups according to the table given in the appendix: B.1 It is clear that there is significant changes for groups that are short lived at small times. This is further confirmation that EDM supports a change in modeling the problematic short-lived isotopes. Once this is combined and updated with all 271 precursors, an even greater effect could be possible.

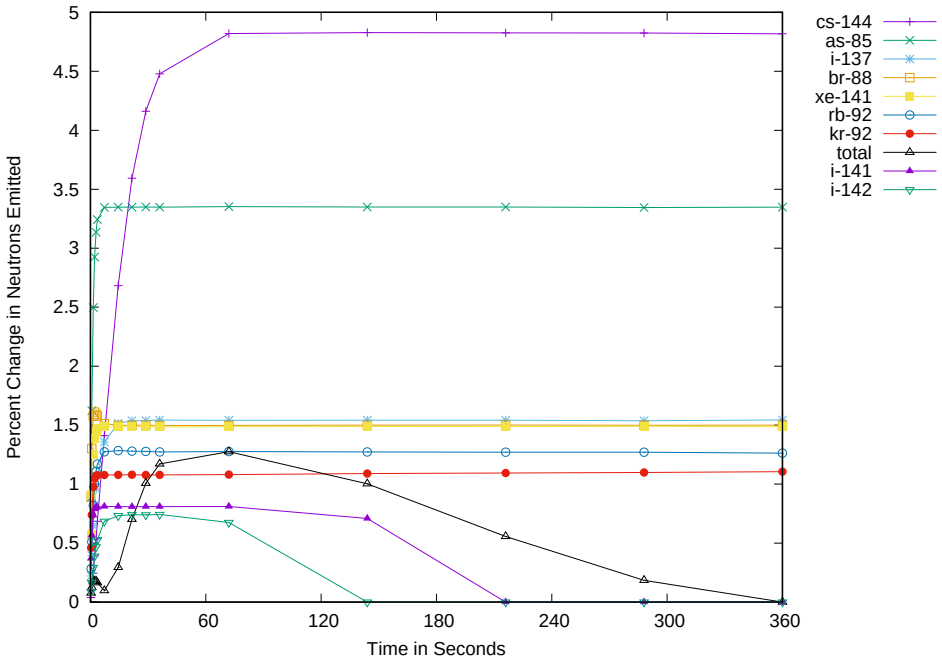

Figure 3.10: Same as 3.9 without ^{146}Cs

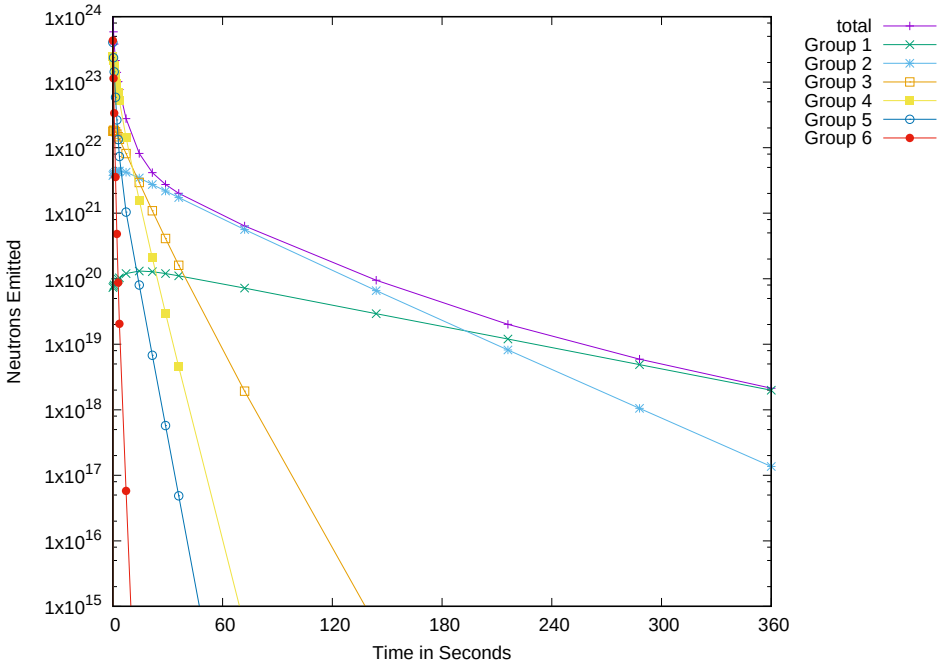

Figure 3.11: All Neutron Emitters Binned into 6 Groups from ^{238}U Burst with ORIGEN

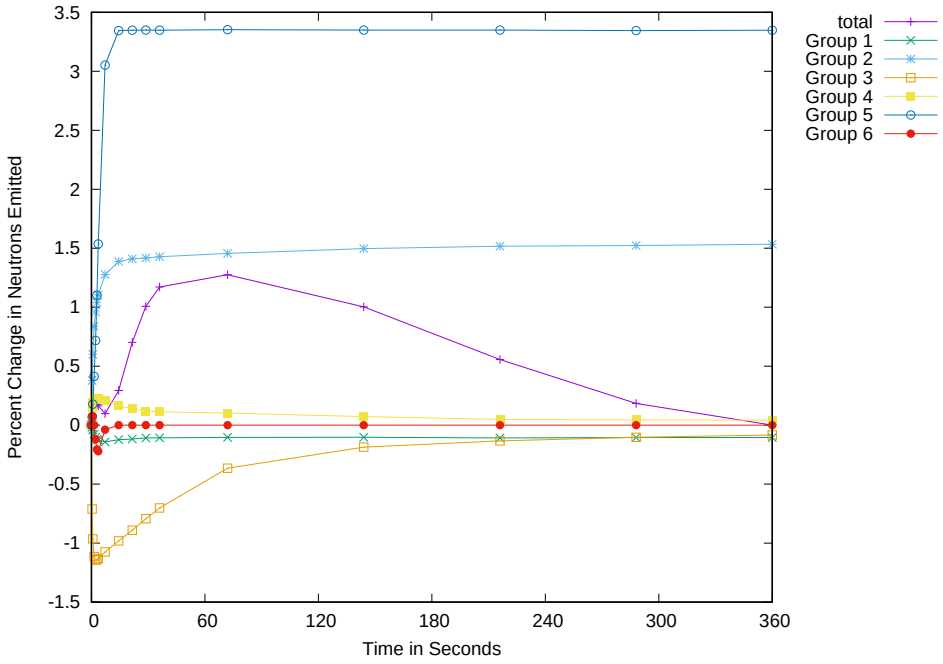

Figure 3.12: % Difference with EDM from ORIGEN for 6 Groups and Total

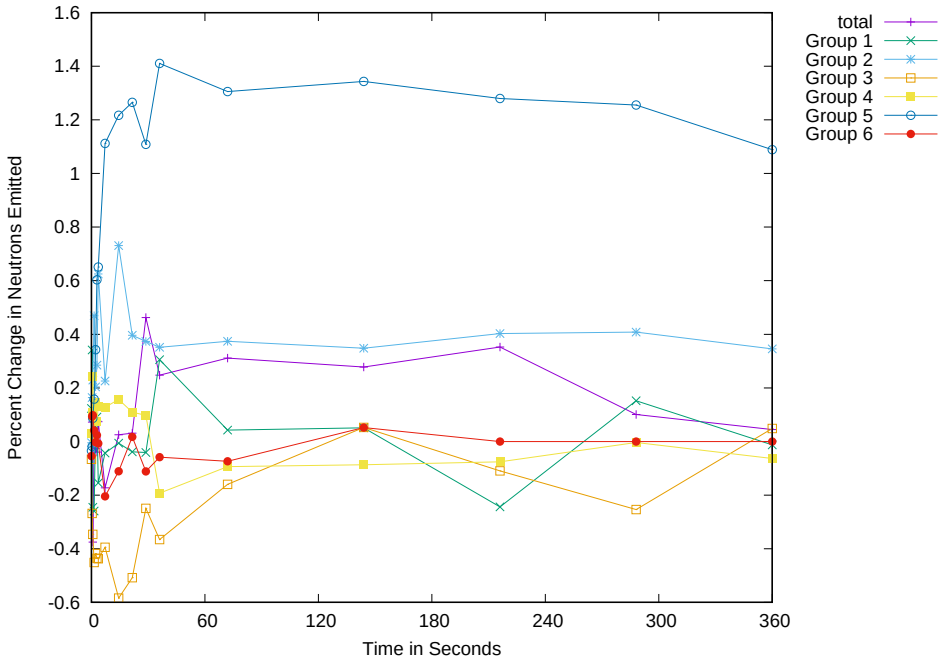

Figure 3.13: % Difference with EDM from ORIGEN for 6 Groups and Total U235

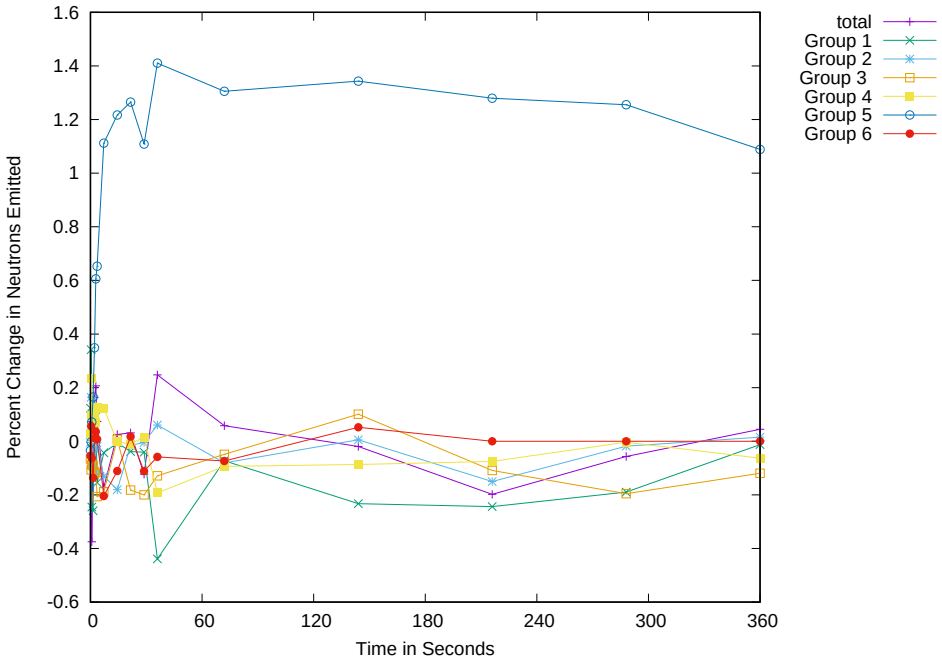

Figure 3.14: % Difference with EDM+EXP from ORIGEN for 6 Groups and Total U235

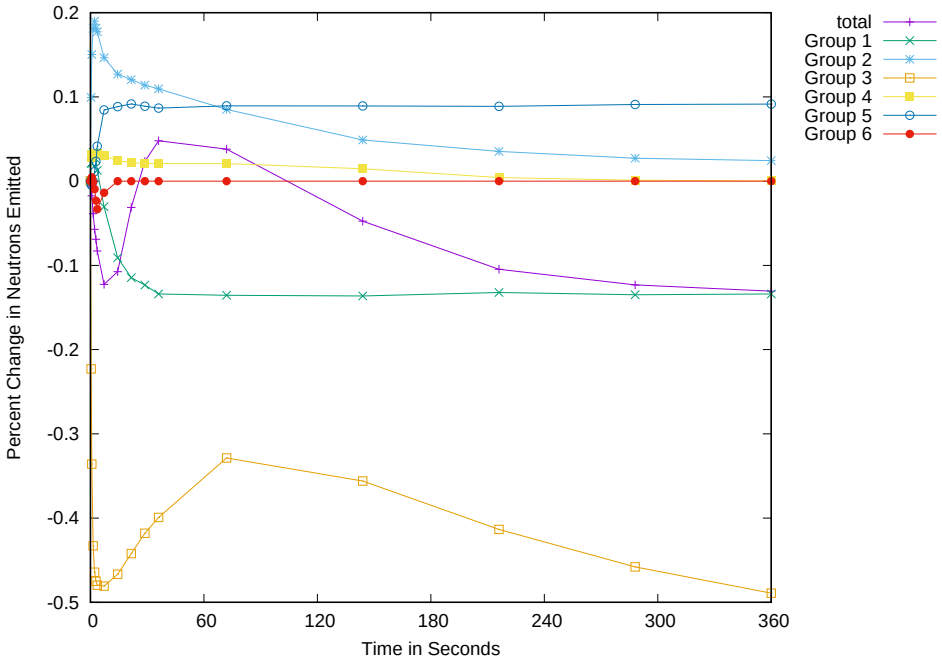

Figure 3.15: % Difference with KHF from ORIGEN for 6 Groups and Total U235

3.5 Discrepancies and Data Errors in ENDF

As mentioned before, there have been many acknowledgments of the limits of the evaluations and data available. In ENDF the cumulative fission product yields have not been updated to include any new decay measurements since ENDF VI. Also, unfortunately some of the yields are dramatically different from other databases available such as the Joint Evaluated Fission and Fusion File (JEFF). While there are many reasons to prefer one database over the other for various applications, it cannot be ignored that the discrepancies can be quite large. In fact if one looks back at the figure with ^{235}U 1.1, one can see some particular features that look out of place. In general when scanning across a particular mass number (A), the magnitude of FPYs should be somewhat Gaussian (large in the middle, low on the edges). One can see this is in fact not the case for several chains. In some cases this may simply be due to some nuclear structure changes as one adds neutrons and protons or transmutations from surrounding nuclei feed a higher yield, so each case would need to be examined individually. One study done by Katakura gives some new fission product yields for three particular nuclei: ^{86}Ge, ^{88}As, and ^{100}Rb [15]. It is very unfortunate that in the case of ^{86}Ge, the difference is simply due to a transcription error! The changes introduced by Katakura change the yields dramatically (2-4 orders of magnitude) which will have very real consequences for several calculations including that of the delayed neutron fraction (DNF).

Many of the P_n yields were not updated to some of the available data as of August 2011. In a soft compilation in 2003 [28], there are at least 126 experimental values of P_n that have a non-zero lower bound, but this is not reflected in the most recent ENDF evaluation of only 97 experimental values. Evaluators of this data said that the original QRPA Hauser-Feshbach calculations for ENDF were done in 2008 and the evaluation was not completed until 2011. They also stated that the QRPA method used experimental data from ENSDF and a few select cases from 2002PF04. In this time there were new experiments, but the data were not updated for a variety of reasons. As of June 2015, ENSDF has 137 isotopes with experimentally determined P_n values that have lower bounds greater than zero and new experimental campaigns are ongoing (data taken from IAEA Nuclear Data Services).

3.5.1 Effects of FPY Changes on Delayed Neutron Fraction of ^{235}U

By adopting the yields for the three nuclei studied by Katakura, we see that the delayed neutron fraction is affected significantly. In current calculations, the total delayed neutron fraction for ^{235}U (as well as other isotopes) is well above the experimentally accepted value. The delayed neutron fraction is defined as:

$$DNF = Yield * P_n \tag{3.3}$$

A more thorough calculation could be carried out to account for the emission of multiple neutrons, but since ORIGEN assumes the P_n is the sum of all subsequent terms, we keep this for EDM as well. Also the time dependence of the total delayed neutron emission for all nuclides can be studied with this approach. This will be done in a later work.

Table 3.17: Delayed Neutron Fraction of Select Isotopes with ENDF Yields for thermal neutron induced fission for ^{235}U

Z	A	ENDF Yield	$Y * Pn_{ENDF}$	$Y * Pn_{EDM}$
Ge	**86**	6.29E-03	3.27E-04	1.32E-03
As	**88**	1.24E-03	5.10E-04	4.75E-04
Rb	**100**	3.48E-04	1.13E-04	1.53E-04
SUMS		7.88E-03	9.50E-04	1.94E-03

Table 3.18: Delayed Neutron Fraction of Select Isotopes for thermal neutron induced fission for ^{235}U with corrected yields as given by Katakura [15]

Z	A	Katakura Yield	$Y * Pn_{ENDF}$	$Y * Pn_{EDM}$
Ge	**86**	3.44E-06	1.79E-07	7.20E-07
As	**88**	1.43E-05	5.88E-06	5.47E-06
Rb	**100**	6.57E-08	2.13E-08	2.90E-08
SUMS		1.78E-05	6.08E-06	6.22E-06

The reason for such a large change with EDM as opposed to ENDF is because the value given for P_n of ^{86}Ge is 0.209 in EDM as opposed to 0.052 in ENDF. There is now experimental data for this that is not in ENDF, which is given to be $P_n = .45 \pm .15$ [25], and which is much

closer to the EDM value as opposed to ENDF. Values of P_n for the other two isotopes are not as disparate and there are still no experimental measurements. Depending upon which model for delayed neutron emission is used this can represent up to a 5 to 10 percent change in the total delayed neutron fraction commonly represented as ν_d.

Chapter 4

Conclusions

4.1 P_n Changes and Consequences

While EDM and QRPA Hauser-Feshbach are different in their approaches (phenomenological vs microscopic), EDM is the clear successor to KHF and is the best global phenomenological approach as of yet when comparing to experimental data. There are also various microscopic approaches that we have studied in this framework, but only one has been presented here. A comparison of P_n data files show that ORIGEN should adopt the multiple neutron emission model of EDM and ENDF experimental data for more consistency. If single neutron emission calculations are used, then the total P_n calculations available from EDM are the clear choice since there will be less inconsistencies built in than by adding in all P_{xn} into the P_n.

4.2 Isotope Changes

Isotope concentrations for the specified nuclei show some variation from the standard ORIGEN calculations in the case of ^{235}U and ^{235}U burst with fast neutrons after 24 hours with both EDM and KHF values for P_n. Isotope concentrations do not differ significantly from the standard ORIGEN calculations with the implementation of EDM and experimental data for P_n from ENDF/B-VII.1 for any of the burst calculations. This could be expected since

the implementation of QRPA Hauser-Feshbach uses a similar level density approximation in the QRPA step. The lack of difference in isotopic concentrations should give users some confidence that the two methods are quite comparable. This result of little change when experimental data is added also extends to the multiple neutron emission calculations for EDM. Different time periods other than 24 hours were not examined in this work, but there is little difference at other time steps except at very short times ($\leq$ 1 hour).

4.3 Delayed Neutron Production

The emitters tracked by the SOURCES 4C code show significant changes in the short lived groups. While more complete calculations need to be done, this is consistent with the prevailing notion that the short-lived isotopes are not well characterized. The need for more experimental data is critical within this region. Older experiments suffered from various flaws that contribute to more uncertainty than even what is stated. Sensitivity studies on neutron production should be made available in later work once uncertainties for theories are developed. We look forward to calculations from Möller and others that will include these uncertainties. ORIGEN is also limited simply by the SOURCES code and its limited number of precursor nuclides that are tracked. It is recommended that the SOURCES code should be updated for ORIGEN and the greater community so that any number of delayed precursors can be tracked explicitly with multiple neutron emissions as well.

4.4 Delayed Neutron Fraction

It is clear that changing the yields of the selected three isotopes influence the total delayed neutron fraction significantly. This further provokes the need for consistent FPYs tied into the decay data. A coordinated research project for FPYs within the IAEA has begun in 2016. We hope the results presented here will help with this effort. More work on FPYs will

be carried out at a later date that is directly related to recomputing cumulative yields using various delayed neutron emission models.

4.5 General Conclusions

The golden standard is experimental results; but because experiments do not exist for all nuclides that are produced from fission, theoretical calculations from the Effective Density Model are employed. The effect of the EDM on nuclide concentrations in the case of all fission bursts presented after 24 hours show little change. However, at shorter time intervals there are significant changes to the isotope concentrations as can be seen by change in the production of delayed neutrons. This work suggests that EDM could be used as a suitable input for decay data when experimental data does not exist, because the neutron emission at short times is positively changed towards the Keepin experimental data from 1997. Also, EDM compares more favorably to experimental data than any of the other phenomenological methods as can be see in table 2.3. EDM should also increase in fidelity as more experimental data is available while methods like QRPA Hauser-Feshbach can only be improved with much more expensive calculations. It is noted that in some locations of the chart, global phenomenological methods fail to reproduce and predict data as well some microscopic theories such as the areas close to shell closures [25].

Since the new decay data are not in sync with the cumulative FPYs in ENDF, several changes need to be made to the independent and cumulative FPYs. Once the most recent experiments done at Holifield and various other facilities around the world are available to evaluations and new FPYs are calculated, the data should be much more reliable. The compilation of that data is taking place in the NDS at the IAEA and results can be found on this website:

$https://www-nds.iaea.org/beta-delayed-neutron/$

4.6 Future Directions

All of the changes in the delayed neutron emitters neutron production was carried out in ORIGEN by calling SOURCES4C which is sorely needing an update. We recommend that this code be updated for ORIGEN to use multiple libraries of delayed neutron emitters using existing data or to create a new code which fulfills the capabilities needed in ORIGEN by SOURCES4C. Since each mass model will yield a different number of precursors, it might be desirable to have a model which is consistent all the way through like those developed from FRLDM. However, it is probably more suitable for practical applications to mix and match theories so as to give reliable results. An example would be to introduce microscopic calculations like NuShellX in the regions or relevance (nuclei near ^{86}Ge) and to use more systematic theories like EDM in areas where microscopic calculations are like to produce irrelevant results [5].

In the endeavor to update SCALE to a new version (6.3), the decay file in ORIGEN is outdated. There is a need for a new format especially given that the uncertainties for experimental data, new spectral data, and multiple neutron emissions are not represented well in the current format. Some work has been done on this by me and is available in the Jupiter cluster at ORNL. It is still a work in progress.

It will be necessary to explore the impact of uncertainty on ORIGEN calculations. The capability already exists with SAMPLER, but uncertainties are not provided by many theories right now (and none that were studied in this work). This is something that could be provided in EDM by recalculating the effective density parameter, a_d, by taking into account the cumulative yields of stable nuclei, which are known to within a few percent. This theory should then be used to recalculate consistent cumulative yields for nuclei that have poor uncertainties on the order of 64% of the total cumulative yield. This could then further be used to calculate a consistent total delayed neutron fraction which this work was unable to do. It will then be possible to truly see the impact of EDM on even more calculations of reactor importance.

No matter what theory or data is chosen for decay data, this work should motivate the need for significant updates to the cumulative FPYs in ENDF. No FPYs should be used without noting the inconsistency between the decay data and the yields. Since FPYs are directly dependent upon this decay data, there needs to be a set of FPYs for each set of data. As such the only consistent data so far is that of ENDF/B-VI.8 which is based on ENDF-349 evaluations.

Bibliography

[1] S. Amiel and H. Feldstein. A semi-empirical treatment of neutron emission probabilities from delayed neutron precursors. *Physics Letters B*, 31(2):59 – 60, 1970. URL: http://www.sciencedirect.com/science/article/pii/0370269370900407, doi:http://dx.doi.org/10.1016/0370-2693(70)90040-7. 14

[2] H. A. Bethe. An attempt to calculate the number of energy levels of a heavy nucleus. *Phys. Rev.*, 50:332–341, Aug 1936. URL: http://link.aps.org/doi/10.1103/PhysRev.50.332, doi:10.1103/PhysRev.50.332. 17

[3] M. Birch, B. Singh, D. Abriola, I. Dillmann, T. D. Johnson, E. A. McCutchan, and A. A. Sonzogni. First Compilation and Evaluation of Beta-Delayed Neutron Emission Probabilities and Associated Half-Lives for A ¡ 72 Nuclei. *Nuclear Data Sheets*, 120:66–69, 2014. URL: http://dx.doi.org/10.1016/j.nds.2014.07.008, doi:10.1016/j.nds.2014.07.008. 10

[4] M. C. Brady. Evaluation and application of delayed neutron precursor data. *LA-11534-T Thesis, Los Alamos National Laboratory*, 1989. 10, 11, 12, 22

[5] B. A. Brown and W. D M Rae. The Shell-Model Code NuShellX@MSU. *Nuclear Data Sheets*, 120:115–118, 2014. URL: http://dx.doi.org/10.1016/j.nds.2014.07.022, doi:10.1016/j.nds.2014.07.022. 19, 54

[6] M. B. Chadwick, M. Herman, P. Obložinský, M. E. Dunn, Y. Danon, A. C. Kahler, D. L. Smith, B. Pritychenko, G. Arbanas, R. Arcilla, R. Brewer, D. A. Brown, R. Capote, A. D. Carlson, Y. S. Cho, H. Derrien, K. Guber, G. M. Hale, S. Hoblit, S. Holloway, T. D. Johnson, T. Kawano, B. C. Kiedrowski, H. Kim, S. Kunieda, N. M. Larson, L. Leal,

J. P. Lestone, R. C. Little, E. A. McCutchan, R. E. MacFarlane, M. MacInnes, C. M. Mattoon, R. D. McKnight, S. F. Mughabghab, G. P A Nobre, G. Palmiotti, A. Palumbo, M. T. Pigni, V. G. Pronyaev, R. O. Sayer, A. A. Sonzogni, N. C. Summers, P. Talou, I. J. Thompson, A. Trkov, R. L. Vogt, S. C. van der Marck, A. Wallner, M. C. White, D. Wiarda, and P. G. Young. ENDF/B-VII.1 nuclear data for science and technology: Cross sections, covariances, fission product yields and decay data. *Nuclear Data Sheets*, 112(12):2887–2996, 2011. doi:10.1016/j.nds.2011.11.002. 2, 4, 26

[7] J K Dickens, T A Love, J W McConnell, J F Emery, K J Northcutt, R W Peelle, and H Weaver. Delayed beta- and gamma-ray production due to thermal-neutron fission of /sup 235/u, spectral distributions for times after fission between 2 and 14,000 sec: tabular and graphical data. Jun 1978. URL: http://www.osti.gov/scitech/servlets/purl/6618867, doi:10.2172/6618867. 3

[8] J. J. Duderstadt and L. J. Hamilton. *Nuclear Reactor Analysis*. Wiley, 1976. xiv, 7, 85

[9] T. R. England, E. D. Arthur, M. C. Brady, and R.J. LaBauve. Background radiation from fission pulses. *LA-11151-MS, Los Alamos National Laboratory*, 1988. URL: http://permalink.lanl.gov/object/tr?what=info:lanl-repo/lareport/LA-11151-MS. 11, 73

[10] T. R. England and B. F. Rider. Evaluation and compilation of fission product yields 1993. *LA-UR-94-3106*, October 1994. 3

[11] M et al. Chadwick. \emph{ENDF/B-VII.0: Next Generation Evaluated Nuclear Data Library for Nuclear Science and Technology}. *emph{Nuclear Data Sheets*}, 107(12):2931–3060, 2006. URL: http://dx.doi.org/10.1016/j.nds.2006.11.001. 15

[12] I. C. Gauld, M. T. Pigni, and G. Ilas. Validation and Testing of ENDF/B-VII Decay Data. *Nuclear Data Sheets*, 120:33–36, 2014. URL: http://dx.doi.org/10.1016/j.nds.2014.06.134, doi:10.1016/j.nds.2014.06.134. 3

[13] A. Gilbert and A. G. W. Cameron. A composite nuclear-level density formula with shell corrections. *Canadian Journal of Physics*, 43(8):1446–1496, 1965. URL: http://dx.doi.org/10.1139/p65-139, arXiv:http://dx.doi.org/10.1139/p65-139, doi:10.1139/p65-139. 17

[14] Walter Hauser and Herman Feshbach. The inelastic scattering of neutrons. *Phys. Rev.*, 87:366–373, Jul 1952. URL: http://link.aps.org/doi/10.1103/PhysRev.87.366, doi:10.1103/PhysRev.87.366. 27

[15] Jun-ichi Katakura, Futoshi Minato, and Kazuya Ohgama. Revision of the jendl fp fission yield data. *EPJ Web of Conferences*, 111:2–7, 2016. xii, 3, 25, 48, 49

[16] T. Kawano, P. Möller, and W. B. Wilson. Calculation of delayed-neutron energy spectra in a quasiparticle random-phase approximation-Hauser-Feshbach model. *Physical Review C - Nuclear Physics*, 78(5):1–8, 2008. doi:10.1103/PhysRevC.78.054601. 3, 10, 22, 26, 27, 68

[17] Toshihiko Kawano and Mark B. Chadwick. Estimation of 239pu independent and cumulative fission product yields from the chain yield data using a bayesian technique. *Journal of Nuclear Science and Technology*, 50(10):1034–1042, 2013. URL: http://dx.doi.org/10.1080/00223131.2013.830580, arXiv:http://dx.doi.org/10.1080/00223131.2013.830580, doi:10.1080/00223131.2013.830580. 3

[18] Kawano, T., Talou, P., and Chadwick, M.B. Monte carlo simulation for statistical decay of compound nucleus. *EPJ Web of Conferences*, 21:04001, 2012. URL: http://dx.doi.org/10.1051/epjconf/20122104001, doi:10.1051/epjconf/20122104001. 27

[19] K. L. Kratz and G. Herrmann. Systematics of neutron emission probabilities from delayed neutron precursors. *Zeitschrift f??r Physik*, 263(5):435–442, 1973. doi:10.1007/BF01391992. 14

[20] Joachim Krumlinde and Peter Mller. Calculation of gamow-teller -strength functions in the rubidium region in the rpa approximation with nilsson-model wave functions.

Nuclear Physics A, 417(3):419 – 446, 1984. URL: http://www.sciencedirect.com/science/article/pii/0375947484904068, doi:http://dx.doi.org/10.1016/0375-9474(84)90406-8. 26

[21] T. Marketin, L. Huther, and G. Martínez-Pinedo. Large-scale evaluation of β-decay rates of r-process nuclei with the inclusion of first-forbidden transitions. *Phys. Rev. C*, 93:025805, Feb 2016. URL: http://link.aps.org/doi/10.1103/PhysRevC.93.025805, doi:10.1103/PhysRevC.93.025805. 14

[22] Catalin Matei, D. W. Bardayan, J. C. Blackmon, J. A. Cizewski, R. K. Grzywacz, S. N. Liddick, W. A. Peters, and F. Sarazin. The versatile array of neutron detectors at low energy (vandle). 2008. 3

[23] E. A. McCutchan, A. A. Sonzogni, T. D. Johnson, D. Abriola, M. Birch, and B. Singh. Improving systematic predictions of β-delayed neutron emission probabilities. *Physical Review C - Nuclear Physics*, 86(4):1–5, 2012. doi:10.1103/PhysRevC.86.041305. 16, 19

[24] K. Miernik. -Delayed Multiple-Neutron Emission in the Effective Density Model. *Physical Review C - Nuclear Physics*, 90(5):1–6, 2014. doi:10.1103/PhysRevC.90.054306. 20

[25] K. Miernik, K. P. Rykaczewski, C. J. Gross, R. Grzywacz, M. Madurga, D. Miller, J. C. Batchelder, I. N. Borzov, N. T. Brewer, C. Jost, A. Korgul, C. Mazzocchi, A. J. Mendez, Y. Liu, S. V. Paulauskas, D. W. Stracener, J. A. Winger, M. Wolińska-Cichocka, and E. F. Zganjar. Large β-delayed one and two neutron emission rates in the decay of Ga86. *Physical Review Letters*, 111(13):1–5, 2013. doi:10.1103/PhysRevLett.111.132502. 4, 10, 11, 18, 19, 20, 24, 49, 53

[26] Peter Mller and Jrgen Randrup. New developments in the calculation of -strength functions. *Nuclear Physics A*, 514(1):1 – 48, 1990. URL: http://www.sciencedirect.

com/science/article/pii/0375947490903300, doi:http://dx.doi.org/10.1016/0375-9474(90)90330-O. 26

[27] P. Möller, A. J. Sierk, T. Ichikawa, and H. Sagawa. Nuclear ground-state masses and deformations: FRDM(2012). *Atomic Data and Nuclear Data Tables*, 109-110:1–204, 2016. URL: http://dx.doi.org/10.1016/j.adt.2015.10.002, arXiv:9308022, doi:10.1016/j.adt.2015.10.002. 4, 65

[28] Bernd Pfeiffer, Karl Ludwig Kratz, and Peter Möller. Status of delayed-neutron precursor data: Half-lives and neutron emission probabilities. *Progress in Nuclear Energy*, 41(1-4 SPEC ISS):39–69, 2002. arXiv:0106020, doi:10.1016/S0149-1970(02)00005-7. 4, 10, 15, 16, 19, 26, 48, 66

[29] M. T. Pigni, M. W. Francis, and I. C. Gauld. Investigation of Inconsistent ENDF/B-VII.1 Independent and Cumulative Fission Product Yields with Proposed Revisions. *Nuclear Data Sheets*, 123:231–236, January 2015. doi:10.1016/j.nds.2014.12.040. 4

[30] Aarno Isotalo; Maria Pusa. Improving the accuracy of the chebyshev rational approximation method using substeps. *Nuclear Science and Engineering*, 183(1), 2016. doi:10.13182/NSE15-67. 21

[31] Peter Ring and Peter Schuck. *The Nuclear Many-Body Problem*. Springer-Verlag Berlin Heidelberg, 1980. 26

[32] G. Rudstam, K. Aleklett, and L. Sihver. Delayed-neutron branching ratios of precursors in the fission product region. *Atomic Data and Nuclear Data Tables*, 53(1):1 – 22, 1993. URL: http://www.sciencedirect.com/science/article/pii/S0092640X83710016, doi:http://dx.doi.org/10.1006/adnd.1993.1001. 25

[33] K. P. Rykaczewski. Decay Studies of 238U Fission Products at the HRIBF (Oak Ridge). *Nuclear Data Sheets*, 120:16–21, 2014. URL: http://dx.doi.org/10.1016/j.nds.2014.06.130, doi:10.1016/j.nds.2014.06.130. 3, 5

[34] Takahiro Tachibana, Masami Yamada, and Yukihisa Yoshida. Improvement of the gross theory of -decay. ii: One-particle strength function. *Progress of Theoretical Physics*, 84(4):641–657, 1990. URL: http://ptp.oxfordjournals.org/content/84/4/641.abstract, arXiv:http://ptp.oxfordjournals.org/content/84/4/641.full.pdf+html, doi:10.1143/ptp/84.4.641. 19

[35] Kohji Takahashi, Masami Yamada, and Takayoshi Kondoh. Beta-decay half-lives calculated on the gross theory. *Atomic Data and Nuclear Data Tables*, 12(1):101 – 142, 1973. URL: http://www.sciencedirect.com/science/article/pii/0092640X73900156, doi:http://dx.doi.org/10.1016/0092-640X(73)90015-6. 14

[36] M. Wang, G. Audi, A.H. Wapstra, F.G. Kondev, M. MacCormick, X. Xu, and B. Pfeiffer. The ame2012 atomic mass evaluation. *Chinese Physics C*, 36(12):1603, 2012. URL: http://stacks.iop.org/1674-1137/36/i=12/a=003. 19, 73

[37] A.H. Wapstra and G. Audi. The 1983 atomic mass evaluation. *Nuclear Physics A*, 432(1):1 – 54, 1985. URL: http://www.sciencedirect.com/science/article/pii/0375947485902830, doi:http://dx.doi.org/10.1016/0375-9474(85)90283-0. 73

[38] A.H. Wapstra, G. Audi, and C. Thibault. The Ame2003 atomic mass evaluation. *Nuclear Physics A*, 729(1):129–336, dec 2003. URL: http://linkinghub.elsevier.com/retrieve/pii/S0375947403018086, doi:10.1016/j.nuclphysa.2003.11.002. 3

[39] W Wieselquist. for High Performance Depletion. *ANS MC2015 JointInternational Conference on Mathematics and Computation (M&C), Supercomputing in NuclearApplications (SNA) and theMonte Carlo (MC) Method*, 2015. URL: http://www.osti.gov/scitech/servlets/purl/1185878. 22, 23

[40] D.H. Wilkinson and B.E.F. Macefield. A parametrization of the phase space factor for allowed -decay. *Nuclear Physics A*, 232(1):58 – 92, 1974. URL: http://www.sciencedirect.com/science/article/pii/0375947474906459, doi:http://dx.doi.org/10.1016/0375-9474(74)90645-9. 17

[41] Justin Willmert and Kemper Talley. Accelerating a metropolis random walk and immersion-method saddle-point algorithms in multidimensional nuclear potential-energy spaces. *LA-UR-13-28028*, pages 323–346, 2013. 2

[42] W. B. Wilson, R. T. Perry, E. F. Shores, W. S. Charlton, Theodore A. Parish, G. P. Estes, T. H. Brown, Edward D. Arthur, Michael Bozoian, T. R. England, and et al. *SOURCES 4C: a code for calculating ([alpha],n), spontaneous fission, and delayed neutron sources and spectra.* Jan 2002. URL: http://www.osti.gov/scitech/servlets/purl/976142. 22

[43] J. A. Winger, S. V. Ilyushkin, K. P. Rykaczewski, C. J. Gross, J. C. Batchelder, C. Goodin, R. Grzywacz, J. H. Hamilton, A. Korgul, W. Królas, S. N. Liddick, C. Mazzocchi, S. Padgett, A. Piechaczek, M. M. Rajabali, D. Shapira, E. F. Zganjar, and I. N. Borzov. Large β-delayed neutron emission probabilities in the ^{78}Ni region. *Phys. Rev. Lett.*, 102:142502, Apr 2009. URL: http://link.aps.org/doi/10.1103/PhysRevLett.102.142502, doi:10.1103/PhysRevLett.102.142502. 4

[44] M. Woliska-Cichocka, K.P. Rykaczewski, A. Fijakowska, M. Karny, R.K. Grzywacz, C.J. Gross, J.W. Johnson, B.C. Rasco, and E.F. Zganjar. Modular total absorption spectrometer at the hribf (ornl, oak ridge). *Nuclear Data Sheets*, 120:22 – 25, 2014. URL: http://www.sciencedirect.com/science/article/pii/S0090375214004487, doi:http://dx.doi.org/10.1016/j.nds.2014.06.131. 3

Appendix

Appendix A

Fission Mass Studies at LANL

All of the work described in the attachment titled: Accelerating a Metropolis random walk and immersion-method saddle-point algorithms in multidimensional nuclear potential-energy spaces, was done in collaboration with Justin Willmert and our mentor Peter Möller. As stated in that report, this author did not have as much coding experience at the time so most of the contributions were made in fine tuning the algorithms and working through the theoretical calculations that would be employed in the revamped code. Specifically, I coded the new method for finding energy minima and worked on providing clearer explanation and framework of the nuclear physics involved so that the code would be faithful to the underpinning theory. The re-development of the saddle-point determination through immersion methods was a joint effort. The parallelization with OpenMP, the idea of simultaneous flooding, and using a bounded-box to restrict flooding were Justin's ideas. All of these things together and their effects on the calculations using the microscopic-macroscopic method are described in the attachment. The attached report was written collaboratively with the writing concerning theory contributed by myself and the writing concerning coding contributed by Justin.

The relevance of those contributions to the present work was a much deeper understanding of microscopic-macroscopic models (FRDM and FRLDM)[27] which are a mass-models for many nuclear calculations including many that are in ENDF. Indeed the KHF calculations

that are mentioned so frequently through this article are intrinsically tied to this mass-model [28].

Appendix B

Different Model Data Comparisons

Before moving on to different models, it is important to point out that a significant collaboration on beta-delayed neutrons has been in progress. The NDS at the IAEA has formed a group that is developing a reference database for Beta-Delayed Neutron Emission. One should familiarize with all of the content on this webpage for more information: https://www-nds.iaea.org/beta-delayed-neutron/

B.1 SOURCES 4C Delayed Neutron

This is the list of 105 delayed neutron emitters in ORIGEN from SOURCES4C and the corresponding half-lives and P_n from 2002PF04. Where possible, experimental data from the 2002PF04 have been reproduced. In cases where it does not exist, the theoretical values from KHF have been placed with the error being specified as theory. Many uncertainties are much larger than the measured value for P_n and as such those quantities might be suspect. These 105 nuclei are not all of the precursors as has been pointed out in the main work. There are more likely to be 200-300 precursors depending on which mass-model is used, but most of the new experimental data is in the higher group numbers which has lower yields and thus will have less contribution to the total number of neutrons measured. A re-measurement of nuclei closer to stability should be a priority since the uncertainties are so high and the

mass-models cannot reproduce some of those neutron emitters, specifically: ^{147}Ba. Also, sometimes the value of Q_β so much lower than S_n of the daughter nucleus that it is hard to believe there are any neutrons emitted at all. ^{103}Nb which has a energy window $(Q_\beta - S_n)$ $474(keV)$ which has a no predicted P_n in KHF and a very low value in EDM (0.00018) and no modern measurements of delayed neutrons, yet it is still included in SOURCES4C and ORIGEN with a value of 0.003 which is a full order of magnitude higher than EDM. ENDF/B-VII.1 gives a value of $\%P_n = 1.18E-6$ from Kawano and Möller Calculations [16] and a cumulative yield of 0.0191189.

Table B.1: 105 Delayed Neutron Emitters from SOURCES4C Coupled with KHF Data Arranged by Group

DNPre	$T_{1/2}$**(ms)**	**Error(ms)**	P_n	**Error**	**Group**
br-87	55600	150	2.52	7	1
cs-141	24940	60	0.038	8	2
i-137	24130	120	7.02	54	2
te-136	17630	80	1.26	20	2
br-88	16360	70	6.55	18	2
sb-134m	10220	90	0.088	17	2
i-138	6490	70	5.17	36	3
rb-93	5840	20	1.44	10	3
se-87	5500	140	0.36	8	3
nb-104	4900	300	0.06	3	3
rb-92	4492	20	0.011	1	3
br-89	4400	30	13.7	4	3
as-84	4020	30	0.18	10	3
la-147	4015	8	0.032	11	3
y-97	3750	30	0.045	20	3
in-127m	3670	40	0.69	4	3

Table **B.1**. Continued.

DNPre	$T_{1/2}$**(ms)**	**Error(ms)**	P_n	**Error**	**Group**
nb-105	2950	60	1.7	9	4
ga-79	2847	3	0.08	14	4
rb-94	2702	5	9.1	11	4
te-137	2490	50	2.86	24	4
i-139	2282	10	10.8	12	4
y-98m	2000	200	3.4	10	4
br-90	1910	10	24.9	10	4
ge-83	1850	60	0.019	theory	4
kr-92	1840	8	0.033	3	4
cs-143	1791	8	1.59	15	4
xe-141	1730	10	0.046	4	4
ga-80	1697	11	0.85	6	4
cs-142	1689	11	0.091	8	4
sb-135	1680	15	22	27	4
se-88	1520	30	0.67	30	4
nb-103	1500	200	0	Theory	4
y-99	1470	7	2.2	5	4
sn-133	1450	30	0.0294	24	4
te-138	1400	400	6.3	21	4
kr-93	1286	10	1.95	11	4
in-129m	1230	30	3.6	4	4
xe-142	1220	20	0.42	3	4
ga-81	1217	5	12.1	4	4
zr-104	1200	300	0.012	Theory	4
y-97m	1170	30	$\leq$0.08	?	4
xe-144	1150	200	0.651	Theory	4

Table **B.1**. Continued.

DNPre	$T_{1/2}$**(ms)**	**Error(ms)**	P_n	**Error**	**Group**
sn-134	1120	80	17	14	4
in-127	1090	10	$\leq$0.03	?	4
la-149	1050	10	1.46	29	4
zn-79	995	19	1.3	4	4
cs-144	993	13	3.41	40	4
ge-84	954	14	10.2	9	4
as-86	945	8	26	7	4
sb-136	923	14	23.2	68	4
tc-110	920	30	0.04	2	4
nb-106	920	40	4.5	3	4
ba-147	893	1	0	Theory	4
tc-109	870	40	0.08	2	4
i-140	860	40	14.4	63	4
kr-95	780	30	4.144	Theory	5
in-128	776	24	0.038	3	5
y-100	735	7	1.16	32	5
sr-98	653	2	0.4	17	5
as-85	650	150	55	14	5
in-129	611	4	0.23	7	5
ba-148	602	25	0.12	6	5
zr-105	600	100	0.127	Theory	5
ga-82	599	2	22.3	22	5
cs-145	582	6	13.1	7	5
as-87	560	110	17.5	25	5
ag-122	550	50	0.186	10	5
y-98	548	2	0.295	33	5

Table **B.1**. Continued.

DNPre	$T_{1/2}$**(ms)**	**Error(ms)**	P_n	**Error**	**Group**
br-91	541	5	31.3	60	5
ge-85	540	50	14	3	5
mo-109	530	60	0.002	Theory	5
la-150	510	30	2.69	34	5
sn-135	450	50	22	7	5
i-141	430	20	30	9	5
sr-97	429	5	0.02	1	5
se-89	410	40	7.8	25	5
rb-95	377.5	8	8.73	31	5
te-139	347	theory	3.304	Theory	5
ba-149	344	7	0.79	39	5
br-92	343	15	33.7	12	5
cd-128	340	30	0.079	theory	5
cs-146	323	6	13.4	10	5
i-142	308	Theory	10.75	Theory	5
ga-83	308	1	38.7	98	5
xe-143	300	30	0.334	Theory	6
mo-110	300	40	0.074	Theory	6
ba-150	300	?	1	5	6
i-143	296	Theory	21.46	Theory	6
ag-123	296	6	0.55	5	6
in-131	280	30	2.2	3	6
in-130	278	3	1.01	22	6
se-91	270	50	21	10	6
sr-99	269	1	0.25	10	6
cs-147	225	5	27.5	21	6

Table **B.1**. Continued.

DNPre	$T_{1/2}$**(ms)**	**Error(ms)**	P_n	**Error**	**Group**
in-132	206	4	5.2	12	6
rb-96	203	3	13.3	7	6
sr-100	202	3	1.11	34	6
kr-94	200	10	5.7	22	6
sb-137	199	theory	25.7	theory	6
rb-97	169.9	7	26	19	6
se-90	161	theory	2.99	Theory	6
br-93	102	10	65	8	6
rb-98	96	3	14.6	18	6
ge-86	95	theory	6.044	theory	6
rb-99	50.3	7	17.3	25	6

B.2 England and Rider Compilation of Delayed Neutron Data

Before the "soft" compilation by Pfieffer et. al was completed, there was extensive work carried out by England and Rider in 1993. The reference includes many important data, but this appendix section serves to present the most important data relevant to this work. It is this work on which cumulative yields of ENDF VI are based. The following table lists $T_{1/2}$, P_n, Uncertainties (dP_n) as well as the group and source for the P_n and mass tables from 3 different tables. The systematic sources are from KHF, but a much older formulation as mentioned in the section about KHF in the main work. M1 is the source of mass of Z,A; M2 source of mass of Z+1,A (beta-decay); M3 is not given in the paper cited, but is given in the following reference as Z+1,A-1 (beta-delayed neutron emission) [9]. W81 and W83 are the Wapstra mass evaluations from 1981 and 1983 [37]. MN means that the Mass Table came from Möller-Nix calculations such as the most recent FRLDM model which was studied in the attached work. Since that time more data has been released in the most recent AME2012 evaluation [36]. One of Möller's models still continues to be used for all nuclei for which we do not have experimental data.

Table B.2: 271 Delayed Neutron Precursors with $T_{1/2}$, P_n, Uncertainties (dP_n) As Found in Table I from LA-UR-86-2693

Nuclide	$T_{1/2}$	$\%P_n$	dP_n	GP	Source	Q_β	S_n	Mass Tables		
								M1	M2	M3
Co-72g	0.1235	11.5322	0	6	sys.	15.03	7.391	MN	MN	MN
Cu-72g	6.4891	0.0001	0	3	sys.	8.964	8.88	MN	W81	W81
Co-73g	0.129	25.122	0	6	sys.	12.8	3.771	MN	MN	MN
Ni-73g	0.4906	0.0047	0	5	sys.	8.17	7.731	MN	MN	MN
Cu-73g	5.1136	0.5588	0	3	sys.	6.174	4.942	MN	W81	W81
Co-74g	0.092	17.4326	0	6	sys.	16.44	6.781	MN	MN	MN

Table **B.2**. Continued.

Nuclide	$T_{1/2}$	$\%P_n$	dP_n	GP	Source	Q_β	S_n	Mass Tables		
								M1	M2	M3
Ni-74g	0.9002	0.356	0	4	sys.	5.98	4.591	MN	MN	MN
Cu-74g	0.6482	0.2949	0	5	sys.	10.221	8.638	MN	W81	W81
Co-75g	0.0817	31.3124	0	6	sys.	14.81	3.451	MN	MN	MN
Ni-75g	0.2312	1.0022	0	6	sys.	9.56	7.031	MN	MN	MN
Cu-75g	0.9274	3.47	0.63	4	meas.	8.055	4.866	MN	W81	W81
Ni-76g	0.3046	3.5113	0	5	sys.	7.7	4.221	MN	MN	MN
Cu-76g	0.2602	2.8418	0	6	sys.	12.004	8.171	MN	W81	W81
Ni-77g	0.1033	4.7115	0	6	sys.	11.05	6.341	MN	MN	MN
Cu-77g	0.3052	12.3119	0	5	sys.	10.185	4.522	MN	W81	W81
Ni-78g	0.1318	9.2984	0	6	sys.	9.07	3.631	MN	MN	MN
Cu-78g	0.1179	9.9093	0	6	sys.	13.673	7.119	MN	W81	W81
Zn-78g	1.9855	0.0041	0	4	sys.	6.01	5.629	W81	W81	W81
Cu-79g	0.1351	24.2057	0	6	sys.	10.77	3.399	MN	MN	W81
Zn-79g	0.313	1.1459	0	5	sys.	9.465	6.854	MN	W81	W81
Ga-79g	3	0.089	0.02	4	meas.	6.77	5.74	W83	W83	W83
Cu-80g	0.0899	15.043	0	6	sys.	16.68	7.181	MN	MN	MN
Zn-80g	0.4873	1.0983	0	6	sys.	7.087	4.803	MN	W81	W81
Ga-80g	1.66	0.83	0.07	4	meas.	10	7.92	W83	W83	W83
Cu-81g	0.0742	52.9504	0	6	sys.	14.9	1.521	MN	MN	MN
Zn-81g	0.1227	5.7372	0	6	sys.	12.125	6.559	MN	W81	W81
Ga-81g	1.23	11.9	0.94	4	meas.	8.32	4.99	W83	W83	W83
Zn-82g	0.1268	21.2264	0	6	sys.	10.42	2.477	MN	MN	W81
Ga-82g	0.6	21.1	1.83	5	meas.	12.993	7.149	MN	W81	W81
Zn-83g	0.0836	22.8749	0	6	sys.	13.71	4.141	MN	MN	MN
Ga-83g	0.31	56.2	9.9	5	meas.	11.97	3.119	MN	MN	W81

Table **B.2**. Continued.

Nuclide	$T_{1/2}$	$\%P_n$	dP_n	GP	Source	Q_β	S_n	Mass Tables		
								M1	M2	M3
Ge-83g	1.9	0.0235	0	4	sys.	8.64	7.88	W83	W83	W83
Ga-84g	0.0984	28.0232	0	6	sys.	15.13	4.971	MN	MN	MN
Ge-84g	1.2	5.2055	0	4	sys.	8.855	4.369	MN	W81	W81
As-84g	5.3	0.086	0.043	3	meas.	9.872	8.681	W83	W83	W83
Ga-85g	0.087	44.9654	0	6	sys.	13.39	2.031	MN	MN	MN
Ge-85g	0.25	16.454	0	6	BETA	11.05	4.226	MN	MN	W81
As-85g	2.03	50	50	4	meas.	8.91	4.54	W83	W83	W83
Ge-86g	0.247	15.2148	0	6	sys.	9.45	2.911	MN	MN	MN
As-86g	0.9	8.503	1.6104	4	meas.	13.372	6.196	MN	W81	W81
Ge-87g	0.1339	15.1329	0	6	sys.	12.61	4.861	MN	MN	MN
As-87g	0.3	44.36	20.217	6	meas.	10.73	2.22	MN	MN	W81
Se-87g	5.6	0.188	0.021	3	meas.	7.17	6.31	W83	W83	W83
Br-87g	55.7	2.54	0.16	1	meas.	6.826	5.515	W83	W83	W83
Ge-88g	0.129	21.6551	0	6	sys.	10.85	2.531	MN	MN	MN
As-88g	0.1348	19.9068	0	6	sys.	13.73	5.531	MN	MN	MN
Se-88g	1.5	0.966	0.021	4	meas.	8.567	4.912	MN	W81	W81
Br-88g	16	6.26	0.38	2	meas.	8.967	7.053	W83	W83	W83
As-89g	0.1212	33.2722	0	6	sys.	11.91	2.761	MN	MN	MN
Se-89g	0.427	7.7	2.4	5	meas.	11.378	5.573	MN	W81	W81
Br-89g	4.38	14	0.84	3	meas.	8.3	5.11	W83	W83	W83
As-90g	0.0911	24.3493	0	6	sys.	15.08	5.291	MN	MN	MN
Se-90g	0.555	9.1321	0	5	sys.	10.204	4.117	MN	W81	W81
Br-90g	1.8	24.6	1.85	4	meas.	10.7	6.31	W83	W83	W83
Se-91g	0.27	24.4382	0	6	sys.	11.25	3.398	MN	MN	W81
Br-91g	0.6	18.1	1.48	5	meas.	11.795	4.493	MN	W81	W81

Table **B.2**. Continued.

Nuclide	$T_{1/2}$	$\%P_n$	dP_n	GP	Source	Q_β	S_n	Mass Tables		
								M1	M2	M3
Rb-91g	58.2	0.0001	0	1	sys.	5.859	5.796	W81	W81	W81
Se-92g	0.1682	13.2333	0	6	sys.	9.48	3.181	MN	MN	MN
Br-92g	0.36	42.7344	9.7464	5	meas.	13.963	5.35	MN	W81	W81
Kr-92g	0.36	0.0332	0.0031	5	meas.	6.156	5.113	W83	W83	W83
Rb-92g	4.53	0.0099	0.0005	3	meas.	8.12	7.366	W83	W83	W83
Se-93g	0.0968	12.0321	0	6	sys.	12.44	5.271	MN	MN	MN
Br-93g	0.176	25.0885	0	6	sys.	12.211	3.518	MN	W81	W81
Kr-93g	1.29	2.01	0.16	4	meas.	8.529	5.914	W83	W83	W83
Rb-93g	5.86	1.35	0.07	3	meas.	7.442	5.237	W83	W83	W83
Br-94g	0.1108	29.8035	0	6	sys.	13.58	4.411	MN	MN	W81
Kr-94g	0.21	6.13	2.41	6	meas.	8.199	4.08	MN	W81	W81
Rb-94g	2.76	10	0.5	4	meas.	10.307	6.786	W83	W83	W83
Br-95g	0.1069	27.0797	0	6	sys.	11.99	3.271	MN	MN	MN
Kr-95g	0.78	7.5051	0	5	BETA	10.078	5.151	MN	W81	W81
Rb-95g	0.38	8.62	0.42	5	meas.	9.282	4.33	W83	W83	W83
Br-96g	0.0888	21.9195	0	6	sys.	14.96	5.491	MN	MN	MN
Kr-96g	0.2931	7.7473	0	6	sys.	8.066	8.066	MN	W81	W81
Rb-96g	0.204	14	0.71	6	meas.	11.75	5.86	W83	W83	W83
Sr-96g	1.1	0.0011	0	4	sys.	5.413	5.176	W81	W81	W81
Kr-97g	0.1	8.3925	0	6	sys.	10.331	5.086	MN	W81	W81
Rb-97g	0.17	26.6	1.48	6	meas.	10.52	3.98	W83	W83	W83
Sr-97g	0.4	0.0054	0.0021	5	meas.	7.47	6.04	W83	W83	W83
Y-97g	3.7	0.054	0.0028	3	meas.	6.68	5.579	W83	W83	W83
Y-97m	1.11	0.109	0.03	4	meas.	0	0	Y97		
Kr-98g	0.1602	8.2989	0	6	sys.	9.48	3.98	MN	W81	W81

Table **B.2**. Continued.

Nuclide	$T_{1/2}$	$\%P_n$	dP_n	GP	Source	Q_β	S_n	Mass Tables		
								M1	M2	M3
Rb-98g	0.11	13.3	1.2	6	meas.	12.43	5.76	W83	W83	W83
Sr-98g	0.65	0.326	0.034	5	meas.	5.88	4.18	W83	W83	W83
Y-98g	2	0.228	0.012	4	meas.	8.918	6.409	W83	W83	W83
Y-98m	0.65	0.228	0.96	5	meas.	0	0	Y98		
Rb-99g	0.145	17.1	4.2	6	meas.	11.32	3.76	W83	W83	W83
Sr-99g	0.6	0.129	0.111	5	meas.	7.95	5.82	W83	W83	W83
Y-99g	1.4	2.02	1.45	4	meas.	7.57	4.552	W81	W81	W81
Rb-100g	0.0984	4.95	1.02	6	meas.	13.733	6.053	MN	W81	W81
Sr-100g	0.618	0.743	0.086	5	meas.	6.7	4.66	W83	W83	W83
Y-100g	0.8	0.842	0.099	5	meas.	9.9	6.95	W83	W83	W83
Rb-101g	0.0939	28.3215	0	6	sys.	12.31	3.178	MN	MN	W81
Sr-101g	0.1941	2.47	0.28	6	meas.	9.026	5.605	MN	W81	W81
Y-101g	0.6071	2.05	0.23	5	meas.	8.72	4.525	W81	W81	W81
Sr-102g	0.2871	4.76	2.29	6	meas.	8.83	5.005	MN	MN	W81
Y-102g	0.9	5.94	1.71	4	meas.	10.442	6.727	MN	W81	W81
Sr-103g	0.1196	8.8758	0	6	sys.	11.59	5.491	MN	MN	MN
Y-103g	0.2604	12.3656	0	6	sys.	8.879	3.929	MN	W81	W81
Zr-103g	1.3377	0.0242	0	4	sys.	7.5	6.839	W81	W81	W81
Nb-103g	1.5	0.0137	0	4	sys.	5.5	5.12	W83	W83	W83
Sr-104g	0.1629	13.4698	0	6	sys.	10.15	3.371	MN	MN	MN
Y-104g	0.1283	8.7769	0	6	sys.	11.89	6.382	MN	MN	W81
Zr-104g	2.573	0.1824	0	4	sys.	5.846	4.728	MN	W81	W81
Nb-104g	4.8	0.0406	0	3	sys.	8.7	7.94	W83	W83	W83
Y-105g	0.1469	19.7529	0	6	sys.	10.43	3.591	MN	MN	MN
Zr-105g	0.493	1.0879	0	5	BETA	8.285	6.03	MN	W81	W81

Table **B.2**. Continued.

Nuclide	$T_{1/2}$	$\%P_n$	dP_n	GP	Source	Q_β	S_n	Mass Tables		
								M1	M2	M3
Nb-105g	2.8	2.2322	0	4	sys.	7	4.73	W83	W83	W83
Y-106g	0.0894	15.6613	0	6	sys.	13.1	5.721	MN	MN	MN
Zr-106g	0.9071	1.5242	0	4	sys.	7.23	4.667	MN	MN	W81
Nb-106g	1	0.9402	0	4	sys.	10.099	7.766	MN	W81	W81
Y-107g	0.0923	25.9442	0	6	sys.	11.7	3.261	MN	MN	MN
Zr-107g	0.243	3.7127	0	6	sys.	9.9	5.931	MN	MN	MN
Nb-107g	0.766	8.7806	0	5	sys.	8.324	4.156	MN	W81	W81
Zr-108g	0.3781	7.0302	0	5	sys.	8.59	3.841	MN	MN	MN
Nb-108g	0.2423	6.4669	0	6	sys.	10.81	6.327	MN	MN	W81
Mo-108g	1.5	0.0001	0	4	sys.	5.251	5.228	MN	W81	W81
Zr-109g	0.13	7.394	0	6	sys.	10.94	5.501	MN	MN	MN
Nb-109g	0.3154	12.6533	0	5	sys.	9.34	4.031	MN	MN	MN
Mo-109g	1.409	0.1359	0	4	sys.	8.189	6.97	MN	W81	W81
Tc-109g	1.4	0.0879	0	4	sys.	5.9	5.18	W83	W83	W83
Nb-110g	0.1298	10.0525	0	6	sys.	11.9	6.121	MN	MN	MN
Mo-110g	2.772	1.3758	0	4	sys.	6.01	3.942	MN	MN	W81
Tc-110g	0.83	0.621	0	4	sys.	9.646	7.689	MN	W81	W81
Nb-111g	0.1718	18.3948	0	6	sys.	10.71	3.781	MN	MN	MN
Mo-111g	0.4664	1.0303	0	5	sys.	8.28	6.051	MN	MN	MN
Tc-111g	1.9824	5.6954	0	4	sys.	8.147	4.552	MN	W81	W81
Mo-112g	0.9754	2.0788	0	4	sys.	7.06	4.321	MN	MN	MN
Tc-112g	0.4314	5.2031	0	5	sys.	10.01	6.184	MN	MN	W81
Mo-113g	0.2287	3.7966	0	6	sys.	9.94	5.911	MN	MN	MN
Tc-113g	0.6524	7.1864	0	5	sys.	8.59	4.491	MN	MN	MN
Ru-113g	3	0.0005	0	4	sys.	7.391	7.185	MN	W81	W81

Table **B.2**. Continued.

Nuclide	$T_{1/2}$	$\%P_n$	dP_n	GP	Source	Q_β	S_n	Mass Tables		
								M1	M2	M3
Tc-114g	0.2023	6.5358	0	6	sys.	11.32	6.511	MN	MN	MN
Ru-114g	8.1365	0.1039	0	3	sys.	5.42	4.54	MN	MN	W81
Rh-114g	1.7	0.002	0	4	sys.	8.263	7.963	MN	W81	W81
Tc-115g	0.2704	14.3371	0	6	sys.	9.93	4.001	MN	MN	MN
Ru-115g	0.8784	0.2276	0	4	sys.	8.17	6.751	MN	MN	MN
Rh-115g	8.3154	0.7746	0	3	sys.	6.405	4.893	MN	W81	W81
Tc-116g	0.1155	12.2226	0	6	sys.	12.67	6.011	MN	MN	MN
Ru-116g	1.7004	1.0811	0	4	sys.	6.73	4.571	MN	MN	MN
Rh-116g	0.9492	0.5379	0	4	sys.	9.417	7.583	MN	W81	W81
Tc-117g	0.1518	21.2499	0	6	sys.	11.01	3.531	MN	MN	MN
Ru-117g	0.3428	2.0509	0	5	sys.	9.48	6.281	MN	MN	MN
Rh-117g	1.2174	4.8201	0	4	sys.	7.53	4.395	MN	MN	W81
Ru-118g	0.6623	4.1092	0	5	sys.	7.8	4.111	MN	MN	MN
Rh-118g	0.3156	2.9167	0	5	sys.	10.38	6.961	MN	MN	MN
Ru-119g	0.195	4.358	0	6	sys.	10.46	6.001	MN	MN	MN
Rh-119g	0.4654	8.2971	0	5	sys.	8.74	4.361	MN	MN	MN
Pd-119g	1.7587	0.0001	0	4	sys.	7.16	7.06	MN	W81	W81
Ag-119g	2.1	0.0001	0	4	sys.	5.37	5.3	W81	W81	W81
Ru-120g	0.3503	7.5652	0	5	sys.	8.94	3.891	MN	MN	MN
Rh-120g	0.1725	5.9282	0	6	sys.	11.59	6.741	MN	MN	MN
Pd-120g	3.9065	0.0068	0	3	sys.	5.687	5.269	MN	W81	W81
Ag-120g	1.17	0.0015	0	4	m$\leq$.003	8.21	8.109	W81	W81	W81
Rh-121g	0.2496	13.5677	0	6	sys.	10.16	4.151	MN	MN	MN
Pd-121g	0.6437	0.2722	0	5	sys.	8.331	6.795	MN	W81	W81
Ag-121g	0.8	0.0753	0.0048	5	meas.	6.4	5.05	W83	W83	W83

Table **B.2**. Continued.

Nuclide	$T_{1/2}$	$\%P_n$	dP_n	GP	Source	Q_β	S_n	Mass Tables		
								M1	M2	M3
Rh-122g	0.1071	8.3012	0	6	sys.	12.9	6.781	MN	MN	MN
Pd-122g	1.4112	0.4377	0	4	sys.	6.28	4.731	MN	MN	W81
Ag-122g	1.5	0.184	0.011	4	meas.	9.427	7.768	MN	W81	W81
Rh-123g	0.1343	17.107	0	6	sys.	10.99	3.961	MN	MN	MN
Pd-123g	0.3004	0.6897	0	5	sys.	9.41	7.091	MN	MN	MN
Ag-123g	0.39	0.545	0.034	5	meas.	7.73	5.394	MN	MN	W81
Pd-124g	0.514	2.6986	0	5	sys.	7.5	4.361	MN	MN	MN
Ag-124g	0.2495	2.2881	0	6	sys.	10.78	7.411	MN	MN	MN
Pd-125g	0.166	2.2664	0	6	sys.	10.31	6.671	MN	MN	MN
Ag-125g	0.3335	6.3167	0	5	sys.	8.83	4.721	MN	MN	MN
Pd-126g	0.252	5.031	0	6	sys.	8.69	4.331	MN	MN	MN
Ag-126g	0.1398	4.638	0	6	sys.	11.5	7.001	MN	MN	MN
Ag-127g	0.1753	9.8629	0	6	sys.	9.84	4.541	MN	MN	MN
Cd-127g	0.5719	0.0101	0	5	sys.	7.72	7.178	MN	W81	W81
In-127g	3.76	0.66	0.063	3	meas.	6.494	5.555	W83	W83	W83
In-127m	1.3	0.0001	0	4	In-127	0	0	In-127		
Ag-128g	0.0943	6.8861	0	6	sys.	12.05	6.691	MN	MN	MN
Cd-128g	1.053	0.1215	0	4	sys.	6.049	5.021	MN	W81	W81
In-128g	0.84	0.061	0.037	4	meas.	9.31	7.88	W83	W83	W83
Cd-129g	0.2987	0.1519	0	6	sys.	8.468	7.14	MN	W81	W81
In-129g	0.99	2.92	0.37	4	meas.	7.6	5.39	W83	W83	W83
In-129m	2.5	0.76	2.5	4	meas.	0	0	In-129		
Cd-130g	0.4767	0.9676	0	5	sys.	7.295	5.029	MN	W81	W81
In-130g	0.58	1.04	0.95	5	meas.	10.2	7.63	W83	W83	W83
In-130m	0.51	1.48	0.105	5	meas.	0	0	In-130		

Table **B.2**. Continued.

Nuclide	$T_{1/2}$	$\%P_n$	dP_n	GP	Source	Q_β	S_n	Mass Tables		
								M1	M2	M3
Cd-131g	0.1062	4.8728	0	6	sys.	12.068	6.635	MN	W81	W81
In-131g	0.28	1.84	1.07	6	meas.	8.82	5.25	W83	W83	W83
In-131m	0.111	1.73	0.24	6	meas.	0	0	In-131		
Cd-132g	0.1357	20.5597	0	6	sys.	11.82	2.893	MN	MN	W81
In-132g	0.12	5.36	0.83	6	meas.	13.235	7.308	MN	W81	W81
In-133g	0.1116	31.656	0	6	sys.	12.6	2.777	MN	MN	W81
Sn-133g	1.47	0.2549	0	4	sys.	9.05	7.38	W83	W83	W83
In-134g	0.0806	33.7565	0	6	sys.	14.74	3.841	MN	MN	MN
Sn-134g	1.04	18.3	13.9	4	meas.	6.925	3.091	MN	W81	W81
Sb-134g	10.2	0.104	0.035	2	meas.	8.41	7.5	W83	W83	W83
Sn-135g	0.418	9.2929	0	5	sys.	9.58	4.507	MN	MN	W81
Sb-135g	1.82	17.87	2.16	4	meas.	7.54	3.51	W83	W83	W83
Sn-136g	0.7172	16.3918	0	5	sys.	8.3	2.431	MN	MN	MN
Sb-136g	0.82	28.9788	3.1138	4	meas.	9.611	4.642	MN	W81	W81
Te-136g	19	1.14	0.43	2	meas.	5.1	3.76	W83	W83	W83
Sb-137g	0.478	18.0322	0	5	sys.	9.02	3.27	MN	MN	W81
Te-137g	3.5	2.69	0.63	3	meas.	7.02	5.07	W83	W83	W83
I-137g	24.5	6.97	0.42	2	meas.	5.885	4.025	W83	W83	W83
Sb-138g	0.1734	22.0114	0	6	sys.	11.61	4.371	MN	MN	MN
Te-138g	1.6	6.78	2.26	4	meas.	6.432	3.913	MN	W81	W81
I-138g	6.5	5.38	0.43	3	meas.	7.82	5.82	W83	W83	W83
Sb-139g	0.2178	41.6934	0	6	sys.	9.64	1.721	MN	MN	MN
Te-139g	0.58	7.9624	0	5	sys.	9.321	4.61	MN	W81	W81
Te-140g	0.8038	15.4961	0	4	sys.	7.36	2.24	MN	MN	W81
I-140g	0.86	9.27	0.79	4	meas.	9.967	5.392	MN	W81	W81

Table **B.2**. Continued.

Nuclide	$T_{1/2}$	$\%P_n$	dP_n	GP	Source	Q_β	S_n	Mass Tables		
								M1	M2	M3
Te-141g	0.2726	10.4723	0	6	sys.	10.05	4.491	MN	MN	MN
I-141g	0.46	21.3	3.2	5	meas.	8.892	3.417	MN	W81	W81
Xe-141g	1.72	0.0353	0.0061	4	meas.	6.155	5.51	W83	W83	W83
Cs-141g	24.9	0.0474	0.055	2	meas.	5.256	4.548	W83	W83	W83
Te-142g	0.5901	15.079	0	5	sys.	8.33	2.581	MN	MN	MN
I-142g	0.2	13.8601	0	6	sys.	11.553	5.242	MN	W81	W81
Xe-142g	1.22	0.404	0.038	4	meas.	5.04	4.146	W83	W83	W83
Cs-142g	1.69	0.0949	0.094	4	meas.	7.32	6.21	W83	W83	W83
I-143g	0.401	38.4989	0	5	sys.	8.9	1.819	MN	MN	W81
Xe-143g	0.96	3.0557	0	4	sys.	8.51	5.289	MN	W81	W81
Cs-143g	1.78	1.6	0.08	4	meas.	6.28	4.24	W83	W83	W83
I-144g	0.146	15.2394	0	6	sys.	11.28	4.971	MN	MN	MN
Xe-144g	1.1	4.6118	0	4	sys.	7.236	3.697	MN	W81	W81
Cs-144g	1.001	3.13	0.17	4	meas.	8.46	5.87	W83	W83	W83
I-145g	0.1934	24.0859	0	6	sys.	9.93	2.93	MN	MN	MN
Xe-145g	0.9	6.109	0	4	sys.	9.191	4.886	MN	W81	W81
Cs-145g	0.59	13.59	0.9	5	meas.	7.8	4.24	W83	W83	W83
Xe-146g	0.5627	6.5048	0	5	sys.	8.122	3.732	MN	W81	W81
Cs-146g	0.34	13.3	1.72	5	meas.	9.41	5.13	W83	W83	W83
Ba-146g	2	0.01	0	4	m≤0.02	4.27	3.77	**		
La-146g	11	0.0035	0	2	m≤.007	6.65	6.591	MN	MN	MN
Xe-147g	0.1991	8.7056	0	6	sys.	10.151	4.81	MN	W81	W81
Cs-147g	0.546	26.1	2.5	5	meas.	8.88	4.24	W83	W83	W83
Ba-147g	1.755	0.021	0.002	4	meas.	5.71	5.67	W83	W83	W83*
La-147g	5	0.033	0.006	3	meas.	5.19	4.48	W83	W83	W83

Table **B.2**. Continued.

Nuclide	$T_{1/2}$	$\%P_n$	dP_n	GP	Source	Q_β	S_n	Mass Tables		
								M1	M2	M3
Cs-148g	0.2056	25.1	2.8	6	meas.	11.777	5.766	MN	W81	W81
Ba-148g	3.325	0.006	0.002	3	meas.	5.4	5.01	W83	W83	W83
La-148g	1.3	0.133	0.01	4	meas.	6.5	6.32	W83	W83	W83
Cs-149g	0.2442	32.7567	0	6	sys.	9.42	2.195	MN	MN	W81
Ba-149g	0.695	0.575	0.084	5	meas.	7.8	5.8	W83	W83	W83
La-149g	2.408	1.06	0.14	4	meas.	6.1	4.95	W83	W83	W83
Cs-150g	0.1238	15.0881	0	6	sys.	11.48	5.021	MN	MN	MN
Ba-150g	0.962	10.9278	0	4	sys.	6.74	2.504	MN	MN	W81
La-150g	0.608	0.3991	0	5	sys.	7.62	6.3	W83	W83	W83
Ba-151g	0.3327	3.7569	0	5	sys.	8.76	5.211	MN	MN	MN
La-151g	0.7194	6.5495	0	5	sys.	7.67	4.089	MN	MN	W81
Ba-152g	0.4205	5.7209	0	5	sys.	7.68	3.681	MN	MN	MN
La-152g	0.285	6.0393	0	6	sys.	9.65	5.661	MN	MN	MN
La-153g	0.3258	10.6885	0	5	sys.	8.64	3.901	MN	MN	MN
Ce-153g	1.4688	0.6219	0	4	sys.	7.04	5.404	MN	MN	W81
La-154g	0.1493	10.2702	0	6	sys.	10.68	5.381	MN	MN	MN
Ce-154g	2.0161	0.6373	0	4	sys.	6.03	4.371	MN	MN	MN
Pr-154g	1.0614	0.111	0	4	sys.	7.575	6.668	MN	W81	W81
La-155g	0.154	16.7592	0	6	sys.	9.6	3.511	MN	MN	MN
Ce-155g	0.5278	1.6004	0	5	sys.	8.05	5.531	MN	MN	MN
Pr-155g	1.1224	1.5427	0	4	sys.	6.79	4.746	MN	MN	W81
Ce-156g	0.5963	2.9922	0	5	sys.	7	3.981	MN	MN	MN
Pr-156g	0.3793	2.717	0	5	sys.	8.78	5.971	MN	MN	MN
Ce-157g	0.2144	4.4528	0	6	sys.	9.05	5.171	MN	MN	MN
Pr-157g	0.38	6.3874	0	5	sys.	7.75	4.141	MN	MN	MN

Table **B.2**. Continued.

Nuclide	$T_{1/2}$	$\%P_n$	dP_n	GP	Source	Q_β	S_n	Mass Tables		
								M1	M2	M3
Pr-158g	0.1685	6.423	0	6	sys.	9.81	5.641	MN	MN	MN
Nd-158g	2.6949	0.0053	0	4	sys.	4.96	4.621	MN	MN	MN
Pr-159g	0.1806	12.3634	0	6	sys.	8.72	3.711	MN	MN	MN
Nd-159g	0.6146	0.2361	0	5	sys.	7.09	5.841	MN	MN	MN
Pm-159g	3.0005	0.0185	0	3	sys.	5.29	4.871	MN	MN	W81
Nd-160g	0.7886	0.9469	0	5	sys.	5.99	4.141	MN	MN	MN
Pm-160g	0.7289	0.2676	0	5	sys.	7.43	6.281	MN	MN	MN
Nd-161g	0.3113	1.6982	0	5	sys.	8.02	5.461	MN	MN	MN
Pm-161g	0.7899	1.7504	0	5	sys.	6.36	4.391	MN	MN	MN
Pm-162g	0.3243	2.1452	0	5	sys.	8.4	5.911	MN	MN	MN
Sm-164g	1.385	0.0124	0	4	sys.	5.01	4.571	MN	MN	MN
Eu-164g	1.5327	0.0001	0	4	sys.	6.59	6.571	MN	MN	MN
Sm-165g	0.4536	0.2491	0	5	sys.	6.93	5.691	MN	MN	MN
Eu-165g	1.3546	0.1911	0	4	sys.	5.65	4.751	MN	MN	MN

** A fictitious S(n) was given this nuclide to obtain a positive energy window. Moeller-Nix masses give a negative energy window, however, this precursor has a measured Pn value.

B.3 Delayed Neutron Fraction in Keepin 6-group Formulation

U^{235}			
Group	Decay constant λ_i (sec^{-1})	Yield (neutrons per fission)	Fraction β_i
1	0.0124	0.00052	0.000215
2	0.0305	0.00346	0.001424
3	0.111	0.00310	0.001274
4	0.301	0.00624	0.002568
5	1.14	0.00182	0.000748
6	3.01	0.00066	0.000273
Total yield: 0.0158			
Total delayed fraction (β):			0.0065

Pu^{239}			
Group	Decay constant λ_i (sec^{-1})	Yield (neutrons per fission)	Fraction β_i
1	0.0128	0.00021	0.000073
2	0.0301	0.00182	0.000626
3	0.124	0.00129	0.000443
4	0.325	0.00199	0.000685
5	1.12	0.00052	0.000181
6	2.69	0.00027	0.000092
Total yield: 0.0061			
Total delayed fraction (β):			0.0021

U^{233}			
Group	Decay constant λ_i (sec^{-1})	Yield (neutrons per fission)	Fraction β_i
1	0.0126	0.00057	0.000224
2	0.0337	0.00197	0.000777
3	0.139	0.00166	0.000655
4	0.325	0.00184	0.000723
5	1.13	0.00034	0.000133
6	2.50	0.00022	0.000088
Total yield: 0.0066			
Total delayed fraction (β):			0.0026

Figure B.1: Historical Keepin 6-group formulation for ENDF/B-IV found in Duderstadt and Hamilton's Reactor Analysis [8]

Appendix C

Fallout Nuclides used for Isotopic Analysis

This table was provided by Brandon Grogan (ORNL) for use in identifying the important fallout isotopes produced after fission bursts. Only the isotope was extracted for use.

Table C.1: Fallout Data

Isotope	Energy	Intensity (cps)	Score	Peak Fraction	Spectrum
Ag-112	617.40	4.18E+03	1.67E+02	0.955	Pu239HE-1d
Ag-112	1387.70	2.60E+02	5.81E+01	0.99	Pu239HE-1d
Ag-112	1613.60	1.21E+02	4.46E+01	1	Pu239HE-1d
Ba-139	165.86	8.18E+03	1.66E+02	0.951	Pu239F-1hr
Ba-140	162.66	4.66E+03	6.74E+01	0.989	U235F-1wk
Ba-140	304.83				Manual
Ba-140	423.72	1.26E+03	3.26E+01	0.991	U235F-1wk
Ba-140	437.58	7.49E+02	2.00E+01	0.976	U235F-1wk
Ba-140	537.26	7.94E+03	2.65E+02	0.978	U235F-1wk
Br-84	1897.60	2.36E+02	3.68E+01	0.992	U235HE-1hr

Table **C.1**. Continued.

Isotope	Energy	Intensity (cps)	Score	Peak Fraction	Spectrum
Cd-117	1303.30	3.87E+02	2.99E+01	0.99	Pu239HE-6hr
Cd-117	1576.60	2.00E+02	2.13E+01	0.992	Pu239HE-6hr
Cd-117m	1997.30	1.45E+02	2.54E+01	0.976	Pu239HE-6hr
Ce-141	145.44	1.78E+04	2.47E+02	1	U235F-1wk
Ce-143	57.36	2.68E+03	3.07E+01	0.999	U235F-3d
Ce-143	293.27	2.68E+04	5.18E+02	0.999	U235F-3d
Ce-143	350.62	1.73E+03	3.81E+01	0.992	U235F-3d
Ce-143	490.37	8.68E+02	2.61E+01	0.962	U235F-3d
Ce-143	664.57	9.35E+02	4.15E+01	0.957	U238F-3d
Ce-143	721.93				Manual
Ce-143	880.46	2.50E+02	1.80E+01	0.977	U235F-3d
Ce-144	80.12				Manual
Ce-144	133.52				Manual
Cs-136+Ba-136m	818.51	2.41E+03	1.51E+02	0.965	Pu239HE-1wk
Cs-136+Ba-136m	1048.10	1.56E+03	1.63E+02	0.995	Pu239HE-1wk
Cs-138	1435.90	8.45E+03	7.63E+02	0.991	U235F-1hr
Cs-138	2218.00	1.16E+03	2.62E+02	0.993	U235F-1hr
Cs-138	2639.60	5.00E+02	1.86E+02	1	U235F-1hr
Eu-155	86.55				Manual
Eu-155	105.31				Manual
I-131	80.18				Manual
I-131	284.31				Manual
I-131	364.49	4.13E+04	9.37E+02	0.98	Pu239HE-1wk
I-131	636.99	2.24E+03	9.35E+01	0.951	Pu239HE-1wk
I-131	722.91				Manual
I-132	262.90	8.32E+02	1.51E+01	0.975	Pu239F-1wk

Table **C.1**. Continued.

Isotope	Energy	Intensity (cps)	Score	Peak Fraction	Spectrum
I-132	284.90				Manual
I-132	505.79	1.82E+03	5.67E+01	0.978	Pu239F-1wk
I-132	522.65	5.74E+03	1.86E+02	1	Pu239F-1wk
I-132	547.20	3.92E+02	1.34E+01	0.997	Pu239F-1wk
I-132	621.20	4.64E+02	1.87E+01	0.966	U235F-1wk
I-132	630.19	4.07E+03	1.67E+02	1	Pu239F-1wk
I-132	650.50	7.63E+02	3.28E+01	0.983	Pu239F-1wk
I-132	667.71	2.87E+04	1.28E+03	0.999	Pu239F-1wk
I-132	669.80	1.35E+03	6.04E+01	0.993	Pu239F-1wk
I-132	671.40	9.99E+02	4.51E+01	0.996	Pu239F-1wk
I-132	727.00	5.87E+02	2.99E+01	0.999	Pu239F-1wk
I-132	727.20	8.53E+02	4.36E+01	0.999	Pu239F-1wk
I-132	728.40	4.26E+02	2.18E+01	0.997	Pu239F-1wk
I-132	772.60	1.94E+04	1.10E+03	0.974	Pu239F-1wk
I-132	809.50	6.32E+02	3.88E+01	0.989	Pu239F-1wk
I-132	812.00	1.36E+03	8.38E+01	0.963	Pu239F-1wk
I-132	863.30				Manual
I-132	876.60				Manual
I-132	910.10				Manual
I-132	954.55	3.75E+03	3.19E+02	1	Pu239F-1wk
I-132	984.20	1.23E+02	1.12E+01	0.999	Pu239F-1wk
I-132	1035.00	1.02E+02	1.04E+01	0.986	Pu239F-1wk
I-132	1136.00	5.54E+02	7.05E+01	1	Pu239F-1wk
I-132	1143.30	2.47E+02	3.20E+01	0.973	Pu239F-1wk
I-132	1148.20				Manual
I-132	1172.90	1.94E+02	2.69E+01	0.997	Pu239F-1wk

Table **C.1**. Continued.

Isotope	Energy	Intensity (cps)	Score	Peak Fraction	Spectrum
I-132	1290.80	1.85E+02	3.33E+01	0.967	Pu239F-1wk
I-132	1295.10	3.08E+02	5.60E+01	0.996	Pu239F-1wk
I-132	1372.10	3.86E+02	8.32E+01	1	Pu239F-1wk
I-132	1398.60	1.08E+03	2.47E+02	1	Pu239F-1wk
I-132	1442.60	2.10E+02	5.30E+01	1	Pu239F-1wk
I-132	1921.10	1.44E+02	1.06E+02	1	Pu239F-1wk
I-132+I-132m	667.71	6.19E+03	2.27E+02	0.971	U235HE-6hr
I-133	510.53	8.39E+02	2.64E+01	0.964	Pu239F-1d
I-133	529.87	3.87E+04	1.27E+03	0.99	Pu239F-1d
I-133	706.58	3.43E+02	1.67E+01	0.967	U235F-3d
I-133	1236.40	3.09E+02	4.92E+01	0.957	U235F-1d
I-134	135.40	1.59E+03	3.11E+01	0.975	U235F-6hr
I-134	595.36	1.67E+03	5.60E+01	0.984	U235F-6hr
I-134	847.02	1.28E+04	5.77E+02	0.973	U235F-1hr
I-134	884.09	6.95E+03	3.28E+02	0.991	U235F-6hr
I-134	1072.50	1.63E+03	9.58E+01	0.995	U235F-1hr
I-134	1613.80	2.74E+02	3.05E+01	0.995	U235F-6hr
I-134	1806.80	3.20E+02	4.48E+01	0.998	U235F-6hr
I-135	288.45	1.96E+03	4.60E+01	0.969	Pu239F-6hr
I-135	417.63	1.61E+03	4.40E+01	0.96	U238F-6hr
I-135	836.80	9.72E+02	6.34E+01	0.965	Pu239F-1d
I-135	1038.80	9.69E+02	9.93E+01	0.997	U235F-1d
I-135	1124.00	7.05E+02	4.41E+01	0.959	U238F-6hr
I-135	1131.50	4.41E+03	2.79E+02	0.983	Pu239F-6hr
I-135	1260.40	5.11E+03	3.75E+02	0.992	Pu239F-6hr
I-135	1457.60	1.36E+03	1.26E+02	0.996	Pu239F-6hr

Table **C.1**. Continued.

Isotope	Energy	Intensity (cps)	Score	Peak Fraction	Spectrum
I-135	1502.80	1.65E+02	1.61E+01	0.996	Pu239F-6hr
I-135	1566.40	1.91E+02	2.01E+01	1	Pu239F-6hr
I-135	1678.00	1.33E+03	1.60E+02	0.999	Pu239F-6hr
I-135	1706.50	5.62E+02	6.99E+01	0.984	Pu239F-6hr
I-135	1791.20	1.02E+03	1.39E+02	0.997	Pu239F-6hr
I-135	2045.90	1.02E+02	1.90E+01	1	Pu239F-6hr
In-117	552.90	6.17E+03	1.97E+02	0.998	Pu239HE-6hr
In-117+In-117m	158.60	1.53E+04	3.07E+02	0.952	Pu239HE-6hr
Kr-87	402.59	3.41E+03	9.14E+01	0.959	U235F-6hr
Kr-87	2554.80	1.64E+02	5.52E+01	0.984	U235HE-1hr
Kr-88	196.30	1.09E+04	2.28E+02	0.996	U235F-6hr
Kr-88	1529.80	8.64E+02	8.72E+01	0.986	U235F-6hr
Kr-88	2029.80	2.81E+02	5.10E+01	0.996	U235F-6hr
Kr-88	2035.40	2.31E+02	4.23E+01	1	U235F-6hr
Kr-88	2195.80	7.63E+02	1.69E+02	0.999	U235F-6hr
Kr-88	2231.80	1.94E+02	4.47E+01	0.994	U235F-6hr
Kr-88	2392.10	1.86E+03	5.18E+02	0.999	U235F-6hr
La-140	328.76	1.07E+04	2.24E+02	1	U235F-1wk
La-140	432.49				Manual
La-140	487.02	1.71E+04	5.09E+02	0.983	U235F-1wk
La-140	751.64	1.12E+03	6.02E+01	0.994	U235F-1wk
La-140	815.77	5.60E+03	3.48E+02	0.999	U235F-1wk
La-140	867.85	1.26E+03	8.77E+01	0.987	U235F-1wk
La-140	919.55	5.77E+02	4.53E+01	0.989	U235F-1wk
La-140	925.19	1.49E+03	1.18E+02	0.995	U235F-1wk
La-140	1596.20	1.29E+04	4.58E+03	1	U235F-1wk

Table **C.1**. Continued.

Isotope	Energy	Intensity (cps)	Score	Peak Fraction	Spectrum
La-140	2521.40	3.15E+02	8.85E+02	1	U235F-1wk
La-142	641.29	7.60E+03	2.70E+02	0.998	U235F-6hr
La-142	894.90	1.00E+03	4.80E+01	0.981	U235F-6hr
La-142	1043.70	2.85E+02	1.62E+01	0.993	U235F-6hr
La-142	1233.10	1.73E+02	1.23E+01	0.983	U235F-6hr
La-142	1545.80	2.25E+02	2.31E+01	0.952	U235F-6hr
La-142	1756.40	1.82E+02	2.40E+01	0.979	U235F-6hr
La-142	1901.30	4.50E+02	7.04E+01	1	U235F-6hr
La-142	2055.20	1.28E+02	2.40E+01	0.997	U235F-6hr
La-142	2187.20	1.88E+02	4.12E+01	0.956	Pu239F-6hr
La-142	2397.80	6.84E+02	1.92E+02	1	U235F-6hr
La-142	2542.70	4.90E+02	1.63E+02	0.999	U235F-6hr
La-142	2971.00	1.34E+02	7.38E+01	1	U235F-6hr
Mo-101	2032.10	1.84E+02	3.36E+01	0.999	Pu239F-1hr
Mo-99	181.07	5.60E+03	8.45E+01	0.98	U235F-3d
Mo-99	739.50	3.79E+03	1.99E+02	1	U235F-3d
Mo-99	777.92				Manual
Nb-95	765.80	9.25E+02	5.15E+01	0.998	U235F-1wk
Nb-97	657.94	3.32E+04	1.45E+03	0.998	U235F-1d
Nb-97m	743.36	2.65E+04	1.40E+03	0.995	U235F-1d
Nd-147	91.11	5.96E+03	7.34E+01	1	U235F-1wk
Nd-147	531.02				Manual
Nd-149	114.31	1.96E+03	3.74E+01	0.989	Pu239F-6hr
Nd-149	155.87	7.84E+02	1.57E+01	0.977	U238F-6hr
Nd-149	270.17	1.11E+03	2.55E+01	0.951	U238F-6hr
Np-239	61.46	1.19E+03	1.38E+01	0.985	U238F-3d

Table **C.1**. Continued.

Isotope	Energy	Intensity (cps)	Score	Peak Fraction	Spectrum
Np-239	104.28	4.90E+04	6.22E+02	0.988	U238F-3d
Np-239	106.12	6.06E+04	7.73E+02	0.998	U238F-3d
Np-239	120.98	1.68E+03	2.22E+01	0.99	U238F-3d
Np-239	121.24	3.44E+03	4.53E+01	0.99	U238F-3d
Np-239	209.75				Manual
Np-239	277.60	3.02E+04	5.65E+02	0.998	U238F-3d
Np-239	285.46				Manual
Np-239	315.88	2.99E+03	6.10E+01	0.98	U238F-3d
Np-239	334.31				Manual
Pm-149	285.80				Manual
Pm-151	167.75	9.20E+02	1.35E+01	0.986	Pu239HE-3d
Pm-151	340.08	1.48E+03	3.19E+01	0.965	Pu239F-1d
Pr-144	696.49				Manual
Pr-144	1489.20				Manual
Pr-146	1524.70	8.00E+02	8.03E+01	0.958	U238F-1hr
Rb-88	898.03	2.05E+03	9.84E+01	0.997	U235F-6hr
Rb-88	1836.00	1.71E+03	2.48E+02	0.999	U235F-6hr
Rb-88	2677.90	1.16E+02	4.51E+01	1	U235F-6hr
Rb-89	1031.90	2.71E+03	1.52E+02	0.951	U235F-1hr
Rb-89	1248.10	1.72E+03	1.25E+02	0.979	U235HE-1hr
Rb-89	2570.20	2.15E+02	7.39E+01	0.999	U235HE-1hr
Rh-105	306.31				Manual
Rh-105	319.23	1.17E+04	2.40E+02	0.981	Pu239F-3d
Rh-105m	129.57	4.64E+03	9.02E+01	0.992	Pu239F-6hr
Ru-103	497.09	1.44E+04	4.40E+02	1	Pu239F-1wk
Ru-103	610.33	7.64E+02	3.00E+01	0.996	Pu239F-1wk

Table **C.1**. Continued.

Isotope	Energy	Intensity (cps)	Score	Peak Fraction	Spectrum
Ru-105	316.44	6.42E+03	1.56E+02	0.969	Pu239F-6hr
Ru-105	393.36	1.81E+03	4.79E+01	0.965	Pu239F-6hr
Ru-105	469.37	7.22E+03	2.09E+02	0.992	Pu239F-6hr
Ru-105	676.36	1.09E+03	4.95E+01	0.964	Pu239F-1d
Ru-105	724.30	1.34E+04	5.24E+02	0.991	Pu239F-6hr
Sb-122	564.24				Manual
Sb-125	427.87				Manual
Sb-125	463.36				Manual
Sb-126	414.70	2.14E+03	5.43E+01	0.999	Pu239HE-1wk
Sb-127	252.40	2.95E+03	5.22E+01	0.966	Pu239HE-1wk
Sb-127	290.80	6.22E+02	1.20E+01	0.964	Pu239HE-1wk
Sb-127	412.10	8.71E+02	2.20E+01	0.962	Pu239HE-1wk
Sb-127	473.00	5.21E+03	1.51E+02	0.99	Pu239HE-1wk
Sb-127	543.30	5.28E+02	1.79E+01	0.977	Pu239HE-1wk
Sb-127	603.50				Manual
Sb-127	685.70	5.40E+03	2.51E+02	0.982	Pu239HE-1wk
Sb-127	783.70				Manual
Sb-128	314.10	4.15E+03	8.42E+01	0.963	Pu239HE-1d
Sb-128	754.00	3.20E+03	1.74E+02	0.986	Pu239HE-1d
Sb-129	683.60	4.50E+02	1.68E+01	0.953	Pu239F-6hr
Sb-129	966.40	8.50E+02	4.42E+01	0.974	U235HE-6hr
Sb-129	1030.10	6.86E+02	3.84E+01	0.96	Pu239F-6hr
Sb-129	1736.50	7.97E+02	1.03E+02	0.999	U235HE-6hr
Sb-130	330.91	3.32E+03	8.17E+01	0.952	Pu239F-1hr
Sb-130+Sb-130m	839.52	3.96E+03	1.77E+02	0.965	Pu239HE-1hr
Sn-125	915.55	1.61E+02	1.25E+01	0.992	Pu239HE-1wk

Table **C.1**. Continued.

Isotope	Energy	Intensity (cps)	Score	Peak Fraction	Spectrum
Sn-125	1067.10	2.00E+02	2.18E+01	0.96	U235HE-1wk
Sn-125	1089.10	1.54E+02	1.76E+01	0.995	Pu239HE-1wk
Sn-127	1095.60	4.78E+02	2.90E+01	0.969	U235HE-6hr
Sn-127	1114.30	9.25E+02	5.72E+01	0.968	U235HE-6hr
Sn-128	482.30	3.33E+03	9.80E+01	0.955	U235HE-1hr
Sr-91	652.90	2.03E+03	8.79E+01	0.969	U235F-1d
Sr-91	749.80	5.31E+03	2.85E+02	0.981	U235F-1d
Sr-91	1024.30	5.75E+03	5.70E+02	0.958	U235F-1d
Sr-91	1280.90	1.32E+02	2.33E+01	0.975	U235F-1d
Sr-91	1413.40	1.28E+02	3.02E+01	1	U235F-1d
Sr-92	1383.90	1.29E+04	1.10E+03	0.994	U235F-6hr
Tc-101	306.83	3.54E+04	8.46E+02	0.993	Pu239F-1hr
Tc-104	358.00	1.62E+04	4.12E+02	0.951	Pu239F-1hr
Tc-104	1596.70	2.10E+02	2.30E+01	0.968	Pu239F-1hr
Tc-99m+Mo-99	140.51	8.40E+04	1.16E+03	0.999	U235F-3d
Te-131+Te-131m	149.71	6.96E+03	9.77E+01	0.986	Pu239HE-3d
Te-131m	200.63	1.49E+03	2.35E+01	0.961	U235HE-3d
Te-131m	452.30				Manual
Te-131m	793.75	1.26E+03	7.45E+01	0.996	Pu239HE-3d
Te-131m	852.21	1.80E+03	1.21E+02	0.97	Pu239HE-3d
Te-131m	1125.50	7.68E+02	9.54E+01	0.966	Pu239HE-3d
Te-131m	1206.60	6.18E+02	9.20E+01	0.996	Pu239HE-3d
Te-132	111.76	1.20E+03	1.55E+01	0.989	Pu239F-1wk
Te-132	116.30	1.39E+03	1.82E+01	0.995	Pu239F-1wk
Te-132	228.16	6.26E+04	1.05E+03	1	Pu239F-1wk
Te-134	201.23	3.92E+03	8.29E+01	0.967	U235F-1hr

Table **C.1**. Continued.

Isotope	Energy	Intensity (cps)	Score	Peak Fraction	Spectrum
U-237	59.54	5.27E+04	6.05E+02	0.999	U238HE-1wk
U-237	64.83	2.51E+03	2.91E+01	0.994	U238HE-1wk
U-237	97.50	5.60E+04	7.00E+02	1	U238HE-1wk
U-237	101.57	9.65E+04	1.22E+03	0.994	U238HE-1wk
U-237	113.83	1.26E+04	1.63E+02	1	U238HE-1wk
U-237	114.78	2.50E+04	3.25E+02	0.985	U238HE-1wk
U-237	164.61	9.29E+03	1.35E+02	0.996	U238HE-1wk
U-237	208.00	1.04E+05	1.67E+03	1	U238HE-1wk
U-237	267.54	2.82E+03	5.16E+01	0.963	U238HE-1wk
U-237	332.35	3.94E+03	8.33E+01	0.981	U238HE-1wk
U-239	74.66	3.27E+04	5.96E+02	0.985	U238F-1hr
Xe-133	81.00	3.30E+04	3.97E+02	0.973	U235F-1wk
Xe-135	249.79	1.11E+05	1.95E+03	1	Pu239F-1d
Xe-135	608.18	1.66E+03	6.50E+01	0.973	Pu239F-1d
Xe-135m	526.56	5.22E+03	1.62E+02	0.96	Pu239F-6hr
Xe-138	1768.30	4.38E+02	5.85E+01	0.965	U235F-1hr
Y-91m	555.57	1.78E+04	6.18E+02	0.998	U235F-1d
Y-92	448.50	1.25E+03	3.54E+01	0.993	U235F-6hr
Y-92	561.10	1.06E+03	3.43E+01	0.989	U235F-6hr
Y-92	934.47	3.96E+03	1.99E+02	0.994	U235F-6hr
Y-92	1405.40	9.60E+02	8.37E+01	0.971	U235F-6hr
Y-93	266.90	4.58E+03	8.37E+01	0.974	U235F-1d
Y-93	947.10	4.40E+02	3.67E+01	0.963	U235F-1d
Y-93	1917.80	1.77E+02	1.29E+02	1	U235F-1d
Y-94	550.90	6.10E+02	1.95E+01	0.956	U235F-1hr
Y-94	918.74	4.46E+03	2.19E+02	0.984	U235F-1hr

Table **C.1**. Continued.

Isotope	Energy	Intensity (cps)	Score	Peak Fraction	Spectrum
Y-94	1671.40	1.17E+02	1.40E+01	0.972	U235F-1hr
Zr-95	724.19				Manual
Zr-95	756.73	3.82E+03	2.08E+02	1	U235F-1wk
Zr-97	355.40	1.12E+03	2.50E+01	0.972	U235F-1d
Zr-97	703.76	3.02E+02	1.46E+01	0.959	U235F-1d
Zr-97	1021.20	2.19E+02	2.16E+01	1	U235F-1d
Zr-97	1276.10	1.68E+02	2.92E+01	0.997	U235F-1d
Zr-97	1362.70	1.73E+02	3.64E+01	0.999	U235F-1d
Zr-97	1750.20	1.48E+02	7.43E+01	0.991	U235F-1d

C.1 Sample ORIGEN Input

This is the ORIGEN input that was used for a ^{238}U fast neutron fission burst. The ORIGEN 6.1 manual can be used to interpret this input.

```
=shell
cp $RTNDIR/fast_mod.f33 .
end

=origens
scale62fido
3$$ 1 1 e 4$$  0 1  e
4$$ a4  0 2  e
7$$ a2 4 e
t
fast_mod.f33
56$$ 35 1 -1 0 -1 a9 0 1 0 3 1 e
t
u238 fast fiss fallout release
' power 4.184E12 MW is scaled to correct for 181.8 vs 200 MeV/fis
59**  1.9623E+29 f0 e
' times are in hours
60** 2.7778e-10 0.0001 0.0002 0.0004 0.0006 0.0008 0.001 0.002 0.004
0.006 0.008 0.01 0.02 0.04 0.06 0.08 0.1 0.2 0.4 0.6 0.8 1.0 1.5 2.0
4.0 6.0 8.0 10.0 12.0 14.0 16.0 18.0 20.0 22.0 24.0
61** f1e-14
67$$ a21 1 1  a41 1 1  a61 1 1  e
68$$ a2 1 e
73$$ 922380
74** 1000.0
75$$ 2
80$$  f1
t
fast_mod.f71
end

=shell
cp fast_mod.f71 $RTNDIR
end
```

Appendix D

EDM Data

The EDM data can be found on github: $https://github.com/kmiernik/delayed_neutrons/blob/master/predictions_total.txt$

Vita

Kemper Dyar Talley was born in Easley, South Carolina to Wayne and Cindy Talley. His love for learning has been lifelong, and his pursuit of physics started at the South Carolina Governor's School for Science and Mathematics under Dr. Mark Godwin. In his undergraduate career at Clemson University, he published 5 first author papers in the area biophysics under Emil Alexov. In his final year he took up an interest in nuclear engineering in physics. After graduation, he received a National Science Foundation Graduate Research Fellowship and entered The Bredesen Center at the University of Tennessee, Knoxville with the intent to study proteins using neutron crystallography at the SNS. However, after meeting and talking with Witek Nazarewicz; he decided to pursue nuclear physics and engineering.